Ab initio calculations of the intermolecular chemical shift in nuclear magnetic resonance in the gas phase and for adsorbed species

Cynthia J. Jameson and Angel C. de Dios
Department of Chemistry, University of Illinois at Chicago, Chicago, Illinois 60680

(Received 9 December 1991; accepted 19 March 1992)

The chemical shifts observed in nuclear magnetic resonance experiments are the differences in shielding of the nuclear spin in different electronic environments. These are known to depend on intermolecular interactions as evidenced by density-dependent chemical shifts in the gas phase, gas-to-liquid shifts, and adsorption shifts on surfaces. We present the results of the first *ab initio* intermolecular chemical shielding function calculated for a pair of interacting atoms for a wide range of internuclear separations. We used the localized orbital local origin (LORG) approach of Hansen and Bouman and also investigated the second-order electron correlation contributions using second-order LORG (SOLO). The ^{39}Ar shielding in Ar_2 passes through zero at some very short distance, going through a minimum, and asymptotically approaches zero at larger separations. The ^{21}Ne shielding function in Ne_2 has a similar shape. The Drude model suggests a method of scaling that portion of the shielding function that is weighted most heavily by $\exp[-V(R)/kT]$. The scaling factors, which have been verified in the comparison of ^{21}Ne in Ne_2 against ^{39}Ar in Ar_2 *ab initio* results, allows us to project out from the same ^{39}Ar in Ar_2 *ab initio* values the appropriate ^{129}Xe shielding functions in the Xe–Ar, Xe–Kr, and Xe–Xe interacting pairs. These functions lead to temperature-dependent second virial coefficients of chemical shielding which agree with experiments in the gas phase. *Ab initio* calculations of ^{39}Ar shielding in clusters of argon are used to model the observed ^{129}Xe chemical shifts of Xe, Xe_2,...,Xe_8 trapped in the cages of zeolite NaA.

I. INTRODUCTION

The nuclear magnetic resonance (NMR) frequency of a nuclear spin in a molecule placed in an external magnetic field depends on the external field, modified by the electrons within the molecule. In an external field $\mathbf{B}_0$, the local field seen by the nucleus is given by

$$\mathbf{B}_{\text{loc}} = (1-\sigma)\mathbf{B}_0. \tag{1}$$

In general, the magnetic field generated by the electrons in the molecule is such as to oppose the applied field, hence the name nuclear magnetic shielding for the second rank tensor quantity σ in Eq. (1). If the molecule is free to tumble, only an isotropic value σ manifests itself. One observes a different resonance frequency for each chemical environment, thus, the difference in shielding between a reference molecule and the molecule of interest ($\sigma_{\text{ref}} - \sigma$) is known as a chemical shift.

Excepting molecular beam studies, the application of NMR to the elucidation of molecular structure and mechanisms of molecular reactions nearly always involves observations of the molecules in some medium, whether in gas, liquid, solid, or adsorbed phases. An understanding of the intermolecular effects on nuclear magnetic shielding is crucial to taking proper account of solvent effects, or conversely, to using the NMR chemical shift as a probe of intermolecular interactions. There is a large body of gas phase data[1,2] which provide information on the intermolecular contributions to the chemical shift; the observed signs, magnitudes, and the dependence on temperature need to be accounted for. NMR is being increasingly used to study adsorbed species.[3,4] At the present time, these studies are largely empirical. An understanding of the signs, the magnitudes of the shifts of adsorbed species relative to the free molecule, their dependence on pore size, sorbate loading, temperature, and the number and positions of counterions is essential for intelligent use of the NMR shifts of adsorbates as a probe of microporous solids such as catalytic materials.

The study of the intermolecular shielding function, the change in the nuclear shielding as a function of the distance between interacting molecules, and their orientation is of fundamental importance in its own right. The intermolecular shielding function in general has important dependence on orientations of the interacting molecules. However, we start with the simplest case of two interacting rare gas atoms and focus attention on the dependence of the shielding on the intermolecular separation R. Therefore, within this article, we will refer to the intermolecular shielding function as $\sigma(R)$.

In principle, the behavior of the intermolecular shielding function of two rare gas atoms at the two limits is well known. The separated atoms is the reference limiting situation; the diamagnetic shielding in a free atom is well known. When the interacting atoms correlate with a united atom S state, as Ar + Ar does with the Kr ground state, the shielding of the united atom is also well known—a purely diamagnetic shielding. Thus, $[\sigma(R) - \sigma(\infty)]$ the intermolecular shielding relative to the separated system for Ar–Ar is known to be $[\sigma(\text{free Kr atom}) - \sigma(\text{free Ar atom})]$ at $R = 0$, and is known to be zero at $R = \infty$. In the intermediate region, the general shape of the function is unknown. We

 0021-9606/92/130417-18$06.00

have suggested for some time that the intermolecular shielding function has the same shape as the intramolecular shielding function for H_2^+, which has been calculated over a wide range of separations,[5] a shape not unlike the shape of the intermolecular energy of interaction for two rare gas atoms. Indeed, there was an indication that there exists a minimum in the function—the result of the direct inversion of the linear density-dependent part of the chemical shift of ^{129}Xe in xenon gas. The empirical form of the intermolecular shielding function showed a minimum in the same general vicinity as the well of the intermolecular potential surface.[6] This inversion could not provide a definitive shape of the function since the temperature range was limited. The indeterminate amount of damping required to limit the undesirable oscillations in the empirical function and yet retain information about its general shape led to considerable uncertainty about the location of the minimum and its depth.

There have been several previous attempts to obtain a theoretical intermolecular shielding function.[7–13] Among these are the calculations of ^1H and He shielding in He–H_2,[7] and ^1H and ^{13}C shielding in the CH_4–He and $(CH_4)_2$ systems.[8] Unfortunately, all of these used a conventional coupled Hartree–Fock (CHF) approach with a common gauge origin, leading to substantial errors arising from gauge origin problems. Furthermore, these authors used basis sets which are now seen to be inadequate. It is questionable whether these previous calculations with minimal or double zeta basis functions reflect the behavior of $[\sigma(R) - \sigma(\infty)]$ accurately. It is interesting to note that all these shielding functions are positive at distances close to the Lennard-Jones r_0 [where $V(R) = 0$] for the molecular pair, and uniformly positive for $R > r_0$, the regime of separations from which arise most of the contributions to the intermolecular shielding observed in the gas phase. Other calculations used local gauge origins such as gauge-including atomic orbitals (GIAO) and individual gauge for localized orbitals (IGLO) applied to the $(CH_4)_2$ dimer,[9] ^{13}C and ^{17}O nuclear shielding in CO–He,[10] and in $(H_2)_2$.[11] It is interesting to note that for ^{13}C in $(CH_4)_2$, the shielding function of Jackowski *et al.*[8] is positive at all values of R of interest; at the separation corresponding to the Lennard-Jones r_0 in particular, it is $+20$ ppm (using a minimum basis set) or $+9$ ppm (double zeta), whereas the GIAO calculation using a minimum basis set gave a value of -1 ppm.[9] The latter calculation shows negative shielding throughout, whereas the former is positive throughout for distances $0.7r_0$ and longer. The GIAO calculation for ^{13}C and ^{17}O in CO–He gave an intermolecular shielding function that was monotonically negative at all distances, even with a Slater-type orbital (STO)-3G basis set.[10] These differences raise questions about the qualitative shape of the intermolecular shielding function. Furthermore, none of these calculations showed any indication of how these functions could be consistent with the large positive value expected at the united atom limit for Ar + Ar, for example.

Another fundamental question is, how important are electron correlation contributions to the intermolecular shielding? Since dispersion forces are attributed to electron correlation, is it essential to use correlated wave functions in calculating the intermolecular $\sigma(R)$?

Finally, an understanding of the intermolecular shielding is crucial to the interpretation of the NMR spectroscopy of adsorbed molecules. The chemical shifts of adsorbed species offer important information about the nature of the adsorbed state. The simplest case is provided by ^{129}Xe nuclei of xenon atoms trapped in the perfectly regular alpha cages of the crystallites of zeolite NaA. The trapped clusters Xe, Xe_2, Xe_3 up to Xe_8 have been observed individually in the NMR spectrum.[14] There is a nearly additive intermolecular effect, i.e., the chemical shifts δ_1, δ_2, δ_3, ... are nearly equally spaced by about 20 ppm, the increments only increasing slightly with n. The sign and magnitude of δ_1 (the difference in shielding between a single xenon atom trapped in an alpha cage and a free xenon atom), as well as its temperature dependence, need to be accounted for. Only when this system is fairly well understood will it be possible to interpret the single average signal of an adsorbed xenon atom whose NMR chemical shift is reporting a summary of all its encounters with channels or cages of various shapes and occupancies.

Apart from the bulk susceptibility shifts which are present in all samples, there are true intermolecular shifts that can be attributed to polar and hydrogen-bonding effects and magnetic anisotropy of neighbor molecules (as in aromatic solvents). These have well-understood mechanisms[15] and will not be discussed further here. The enigmatic part of the intermolecular shielding is that which gives rise to what has been termed van der Waals shifts.[16] This is the subject of this paper.

II. THE DRUDE MODEL

It was shown by London that all molecules produce fluctuating instantaneous electric fields which average out to zero, but which have a nonzero mean square.[17] Coupled with the early realization that changes in nuclear magnetic shielding will take place when the electron cloud of a molecule is distorted by an external electric field,[18,19] this provides a simple physical picture and a plausible mechanism for intermolecular chemical shifts.[20,21] The simple ideas associated with fluctuating electric dipoles constitute a simple model that simultaneously provides dispersion energies, physisorption energies, and intermolecular shielding of rare gas atoms.

The Drude model considers an atom as being composed of a pair of harmonically and isotropically bound particles of equal, opposite charges.[22] Each atom has three modes of vibration whose frequencies are triply degenerate when isolated. As the two atoms approach each other, these vibrational frequencies are perturbed and the total energy becomes the sum of six terms, one for each mode. The zero point energies in the interacting pair at distance R differs from that in the isolated atom by

$$W = (1/2)\hbar \sum_{i=1}^{6} [\omega_i(R) - \omega_0]. \tag{2}$$

The six eigenfrequencies are

$$\omega_{1,2} = \omega_0 [1 \pm 2\alpha(0)/R^3]^{1/2}, \tag{3}$$

$$\omega_{3,4} = \omega_{5,6} = \omega_0 [1 \pm \alpha(0)/R^3]^{1/2}, \tag{4}$$

where $\alpha(0)$ is the static polarizability of the atom. When $\alpha(0) < R^3$, the square roots can be expanded in powers of $\alpha(0)/R^3$, leading to an expression for W whose dominant term is

$$W = -(3/4)\hbar\omega_0\alpha(0)^2/R^6 + \cdots . \tag{5}$$

For the case of two unlike molecules 1 and 2,

$$W = -(3/2)\hbar \frac{\omega_{01}\omega_{02}}{\omega_{01}+\omega_{02}} \frac{\alpha_1(0)\alpha_2(0)}{R^6}. \tag{6}$$

If the natural frequency of the isolated Drude oscillator is taken to be the ionization potential U, then the same result as the London formula[17,23] for the dispersion energy is obtained

$$W = -(3/2) \frac{U_1 U_2}{U_1+U_2} \frac{\alpha_1(0)\alpha_2(0)}{R^6}. \tag{7}$$

The Drude model also provides a model for the shielding change due to the dispersion interaction, as follows: for a nucleus in a rare gas atom placed in a static electric field F, the shielding change relative to the atom in the absence of the field is[24]

$$\sigma(F) = \sigma(\text{free atom}) - BF^2, \tag{8}$$

where B may be called the shielding hyperpolarizability, which provides the response of the shielding of the atom to the static electric field. For a nucleus in a rare gas atom interacting with another rare gas atom, it was first suggested by Bothner-By[21] and then also by Raynes, Buckingham, and Bernstein[20] that the mean-square electric field due to atom 2 that should be used is $3U_2\alpha_2(0)/R^6$. It has been shown[25,26] that if the response of the shielding to a static electric field is to be used in this context, an effective *static* field squared that is equivalent to the mean-square fluctuating field would be more appropriate. In the Drude model, the effective static field squared at atom 1 due to atom 2 is

$$\overline{F_{\text{eff}}^2} = (3/2) \frac{U_1 U_2}{U_1+U_2} \frac{\alpha_2(0)}{R^6}, \tag{9}$$

which agrees with the London dispersion energy being a sum of the polarization energies of atom 1 and atom 2 in the presence of the mean-square electric field created by each other. Thus, the shielding change of atom 1 relative to the isolated atom caused by the dispersion interaction with atom 2 at distance R is

$$[\sigma(R) - \sigma(\infty)] = -B_1(3/2) \frac{U_1 U_2}{U_1+U_2} \frac{\alpha_2(0)}{R^6}, \tag{10}$$

where B_1 is taken to be the same as the shielding hyperpolarizability for the isolated atom 1 in a static electric field. As in the London dispersion energy, this is only the leading term in the interaction; additional terms in R^{-8} (and R^{-10}) may also be considered. Furthermore, this model is only valid for distances such that $R^3 > \alpha(0)$, where the original expansion of the square root terms in Eqs. (3)–(4) are valid, i.e., for distances where the overlap between the two interacting atoms is negligible. At shorter distances, only a quantum mechanical calculation of the shielding in the supermolecule can provide the correct shielding function.

III. *AB INITIO* CALCULATIONS OF ^{39}Ar AS A MODEL FOR ^{129}Xe

The simplest intermolecular shielding function is that for interacting rare gas atoms; the shielding surface is defined by only one variable, the internuclear separation. Although there are available gas phase data for ^{129}Xe interacting with various molecules, *ab initio* calculations on the xenon system are prohibitive, so we choose a smaller rare gas atom for the chemical shielding calculations. For some observables, the He, Ne set of data for rare gas atoms behaves differently from the Ar, Kr, Xe set of data, therefore, it might not be best to choose the smallest rare gas atoms. We believe that ^{39}Ar serves as a good model system for ^{129}Xe.

Calculations of chemical shielding require reasonably large basis sets (at least triple zeta plus three polarization functions). For the calculation of the intermolecular shielding, it is even more important to damp out the errors which result from incomplete cancellation of large positive and negative long-range contributions. In calculations of magnetic properties, this is known as a gauge origin problem. Furthermore, since the long-range interaction between two rare gas atoms is a result of electron correlation, we need to investigate any additional contributions from electron correlation beyond the coupled Hartree–Fock or random phase approximation (RPA) level of theory. For these reasons, we choose a local origin method that effectively damps out the errors in calculating the long-range contributions to the diamagnetic and paramagnetic terms and which can be extended to include second-order correlation contributions. The localized orbital local origin (LORG) method developed by Hansen and Bouman[27] takes the following approach:

In the calculation of the nuclear magnetic shielding, the computation of the diamagnetic part (entirely dependent on the molecular ground state wave function) and the paramagnetic part (dependent on the mixing of ground and excited states by the magnetic perturbation) leads to an unbalanced treatment of the two terms. It is well known that the incomplete cancellation of long-range contributions to the diamagnetic and paramagnetic terms leads to errors. One way of avoiding such incomplete cancellation is to employ commutation rules and identities which conveniently remove such terms before the computation is carried out. This is the approach of Hansen and Bouman. The equations for the calculation of the remaining terms are the following:

$$\begin{aligned}\sigma_{ij}^{d} = (1/c^2) \sum_{\alpha} \langle\alpha|\{&(\mathbf{r}-\mathbf{R}_\alpha)\cdot\mathbf{r}\delta_{ij} \\ &- [\mathbf{u}_i\cdot(\mathbf{r}-\mathbf{R}_\alpha)](\mathbf{u}_j\cdot\mathbf{r})\}/r^3|\alpha\rangle \\ &+ (i/c^2) \sum_{\alpha m}\sum_{\beta n} [\mathbf{u}_i\cdot\langle\alpha|\mathbf{l}/r^3|\beta\rangle] \\ &\times [\mathbf{u}_j\cdot(\mathbf{R}_\alpha - \mathbf{R}_\beta)\times\langle\beta|\mathbf{r}|\alpha\rangle],\end{aligned} \tag{11}$$

$$\sigma_{ij}^{p} = (-2/c^2) \sum_{\alpha m}\sum_{\beta n} t_{\alpha m}^{(1)}(\mathbf{l}/r^3)\Omega_{\alpha m,\beta n}^{(1)} t_{n\beta}^{(1)}(\mathbf{l}^{(\alpha)}), \tag{12}$$

where $t_{\alpha m}^{(1)}(\mathbf{l}/r^3)$ and $t_{n\beta}^{(1)}(\mathbf{l}^{\alpha})$ are transition moments $\langle\alpha|\mathbf{l}/r^3|m\rangle$ and $\langle n|\mathbf{l}^{\alpha}|\beta\rangle$. The $\Omega^{(1)}$ matrix is of the order $n_{\text{occ}} \times n_{\text{virt}}$ and is constructed using the matrix elements of

the Fock operator and the electron repulsion integrals in the molecular orbital (MO) basis. Orbitals α and β, if directly associated with the NMR nucleus, have the local gauge origin $\mathbf{R}_\alpha$ and $\mathbf{R}_\beta$ at the nucleus in question; distant orbitals have their gauge origins at their orbital centroid positions. $\mathbf{l}^\alpha$ is the electronic angular momentum operator relative to $\mathbf{R}_\alpha$.

This level of computation (RPA) includes in $\Omega^{(1)}_{\alpha m,\beta n}$ matrix elements that are singly and doubly excited with respect to the self-consistent field (SCF) ground state and may be said to contain electron correlation[28] (still a point of disagreement among theoreticians). The advantages of using the Hansen–Bouman approach are further enhanced by the existing code for the extension of their method to include second-order correlation contributions to the shielding. Correlation effects may be included by means of a Møller–Plesset expansion of the ground state.[29] In the second order LORG (SOLO) approach, the energy matrices and transition moments in Eqs. (11) and (12) are evaluated using such an expansion, taking care to retain all terms through second order in electron correlation, i.e., using $\Omega^{(2)}$ and $t^{(2)}$.[30] The second-order effects on the diamagnetic terms have not been included in this calculation. These have been shown to be small, even for molecules such as CO and N_2 for which a correct description requires more than one determinant. For these molecules, the diamagnetic shielding results from configuration interaction (CI) calculations differ by less than 2 ppm from the self-consistent field (SCF) results for all nuclei.[31,32]

We have found in basis set studies in previous calculations using LORG[33,34] that basis sets for atoms in the second row of the Periodic Table should include a standard triple zeta plus three *d* polarization functions in order to achieve acceptable accuracy. Therefore, for this paper, we have used for the argon atom and also for the Na^+ ion a 6-311G(3*d*) basis set. GAUSSIAN 88[35] provided the SCF results to input to the LORG calculations using RPAC 8.5.[36] The same package of programs provided a conventional coupled Hartree–Fock calculation using a common origin, for comparison. The second order polarization propagator approximation (SOPPA) and SOLO calculations were carried out with the help of Professor T. D. Bouman using GAUSSIAN 90 (Ref. 35) to generate the SCF molecular orbitals, and the RPAC 9.0 molecular properties programs system[36] implemented on the Cray 2 of the National Center for Supercomputing Applications at the University of Illinois, Urbana.

The use of counterpoise or ghost orbitals[37] would reduce the bias that results if the pair basis represents the wave function of Ar_2 in the simultaneous fields of the external magnet and the nuclear moment more accurately than the single atom basis represents the wave function of an isolated Ar atom in the presence of the two fields. Since the chemical shielding is a localized property (the shielding field produced by an electron is proportional to the inverse cube of the distance of the electron from the observed nucleus), basis set superposition errors are expected to be negligible even in this case where the intermolecular effects on shielding are being sought. Nevertheless, to verify this expectation, we carried out calculations of the single Ar atom at the 6-311G (3*d*) level with and without an equal number of ghost orbitals at various internuclear distances. We have established that the ghost orbital contribution is entirely negligible in this system.

The LORG results for Ar_2 are shown in Fig. 1. This is the first *ab initio* intermolecular $\sigma(R)$ function that has been calculated for a range of values of internuclear separations wide enough to show the shape of the function, and which is consistent with the correct limit at $R = 0$. The behavior at extremely short distances can become very complicated because of avoided curve crossings with other states of the same symmetry. In any case, these regions are not sampled at the modest temperatures and pressures at which the experiments have been carried out. Thus, we merely indicate the connection to the united atom limit with a dashed curve, making no implications about the actual behavior at these very short distances. In Fig. 2, we show $\sigma(R)$ for Ar_2 in more detail and superimpose on this the Ar–Ar intermolecular interaction potential function $V(R)$ (Ref. 38) to indicate which regions of the $\sigma(R)$ function contribute the most to intermolecular effects in the gas phase. The inset shows the $\sigma(R)$ function in an expanded scale in this region.

In order to determine the additional contributions to the intermolecular shielding due to second-order correlation contributions, we carried out calculations using the SOLO method at selected internuclear separations. The results are shown in Table I, compared with the LORG results at the same internuclear separations.

It can be seen that the differences between the two calcu-

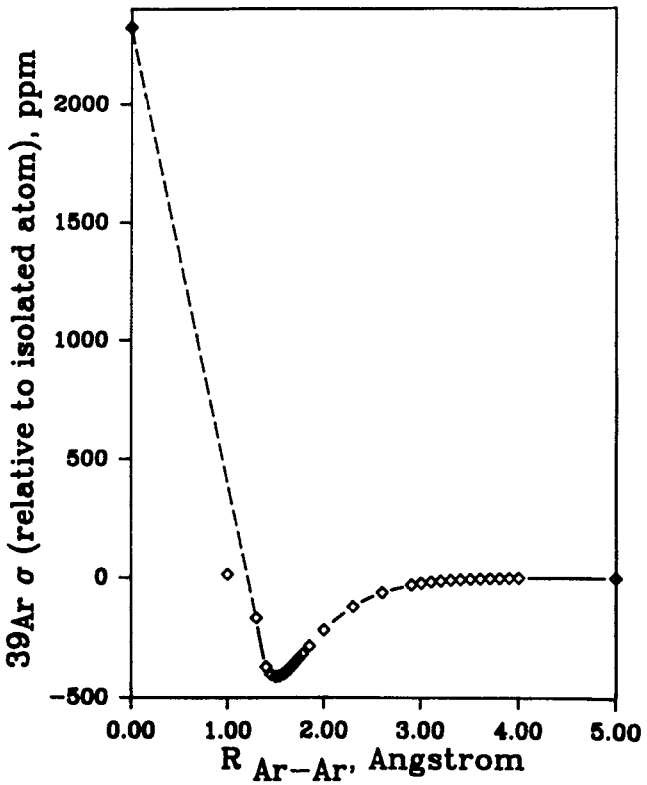

FIG. 1. The ^{39}Ar chemical shielding in Ar–Ar obtained by *ab initio* calculations, in ppm relative to the isolated atom.

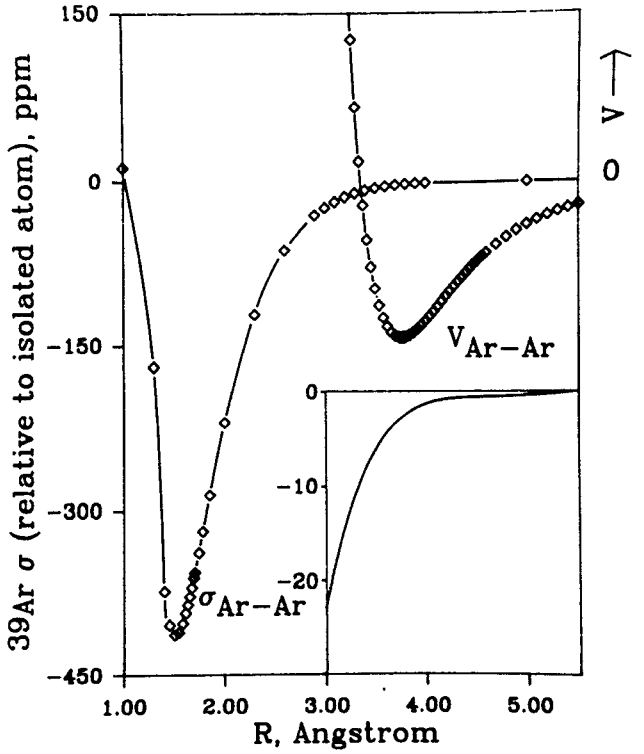

FIG. 2. The ^{39}Ar chemical shielding in Ar–Ar obtained by *ab initio* calculations, in ppm relative to the isolated atom; the inset shows in an expanded scale that region of the shielding function which provides significant contributions for averaging at 100–500 K. The Ar–Ar intermolecular potential function is also shown (Ref. 38), well depth $\epsilon/k = 141$ K, and $V(R) = 0$ at 3.350 Å.

is an S state. The diamagnetic and paramagnetic parts of the shielding can be defined in different ways, depending on the choice of gauge. One commonly used definition is to use the Coulomb gauge and to choose the gauge origin at the nucleus of interest. With the gauge origin at the Ar nucleus of interest, it is possible to approximate the σ^{diam} term by using the Flygare approximation[39]

$$\sigma^{\text{diam}}(^{39}\text{Ar in Ar}_2, R) - \sigma(\text{free Ar atom}) = (e^2/3mc^2)18(1/R). \quad (13)$$

The diamagnetic term in Ar_2 should change monotonically from the united atom value $\sigma(^{83}\text{Kr}$ in the free Kr atom) to $\sigma(^{39}\text{Ar}$ in the free Ar atom), i.e., 3245.6 ppm (Ref. 40) (or 3598 ppm with relativistic corrections)[41] to 1237.64 ppm, taking a roughly $(1/R)$ shape at large R values. Based on symmetry arguments, the paramagnetic term in Ar_2 should be zero at the united atom limit (the spherically symmetric S state of the Kr atom), zero at the free argon atom limit, and negative in between. The sum of $\sigma^{\text{diam}} + \sigma^{\text{para}}$ would then change with internuclear separation in a predictable way as sketched in Fig. 3. Provided that σ^{para} exceeds σ^{diam} as the argon atoms approach from infinite separation, the total intermolecular shielding should be negative at the interesting distances [shown as Fig. 3(a)]. On the other hand [shown as Fig. 3(b)] there may be some systems in which the diamagnetic term σ^{diam} could dominate at the large R values, become equal to the paramagnetic term at some intermediate value, and be overcome by the negative σ^{para} further in. At shorter distances yet, the diamagnetic terms would win

lations are very small for this system; LORG provides nearly as complete answers to the chemical shielding due to van der Waals interactions as does SOLO. It appears that the RPA level of the LORG calculation gives nearly all $\sigma(R)$ due to the induced dipole–induced dipole interactions in this particular system. The second-order electron correlation contributions at short range are also relatively small.

The qualitative shape of the intermolecular $\sigma(R)$ shown in Fig. 1 can be predicted from a consideration of the diamagnetic (σ^{diam}) and the paramagnetic (σ^{para}) terms in the shielding of a rare gas pair for the case where the united atom

TABLE I. Chemical shielding values for ^{39}Ar in Ar_2 at two levels of calculation with (SOLO) and without (LORG) second-order electron correlation.

	$[\sigma(R) - \sigma(\infty)]$ (ppm)	
R (Å)	LORG	SOLO
1.70	− 356.90	− 353.49
2.30	− 121.39	− 119.64
2.90	− 30.32	− 30.68
3.00	− 23.53	− 23.91
4.00	− 1.30	− 1.40
5.00	− 0.04	0.00

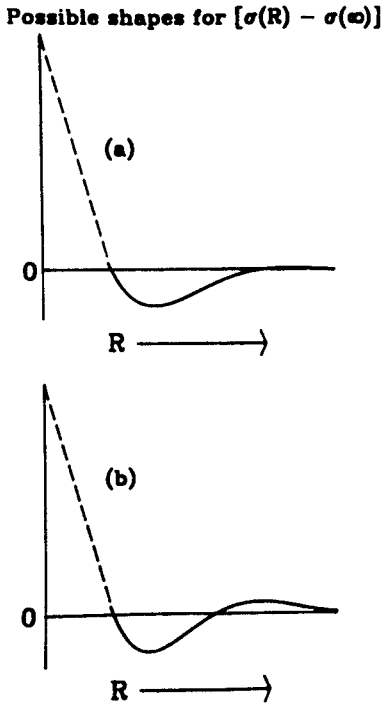

FIG. 3. Sketches of possible shapes of the intermolecular shielding function for interacting rare gas atoms based on a monotonically decreasing $\sigma^{\text{diam}} \propto 1/R$ at large R and symmetry arguments applied to σ^{para}.

out again, leading to a positive net shielding, increasing toward the large positive united atom value. Our *ab initio* calculations reveal behavior type (a) for the ^{39}Ar shielding in the Ar_2 system, but it may be expected that behavior (b) could be observed for ^{1}H shielding. Indeed, the ^{1}H in triplet H_2 shows the (b) type behavior at intermediate and large separations when calculated over a wide range of values of internuclear separations by a density functional method developed by Grayce and Harris.[13] The earlier calculations on this system by Marshall and Pople[42] using the Heitler–London molecular wave function also starts out positive at large separations, crosses the axis, and becomes negative at $4a_0$.

For a more accurate depiction of the σ^{diam} and σ^{para} terms when the gauge origin is placed at the ^{39}Ar nucleus in question, we carried out a calculation of σ^{diam} for Ar_2 using the same basis set as used in Figs. 1 and 2. σ^{diam} is only dependent on the unperturbed electronic wave function of the Ar_2 system, which is easily calculated. The correlation contributions to the diamagnetic terms are known to be negligibly small.[31,32] Since LORG (or SOLO) gives us the sum

$$\sigma(R) = \sigma^{\text{diam}} + \sigma^{\text{para}}, \tag{14a}$$

we can get σ^{para} by difference. These results are shown in Fig. 4. By symmetry, the parallel component of $\sigma(R)$ in Ar_2 is purely diamagnetic and very nearly unchanged from σ(free atom) except at very short distances; the perpendicular component includes nearly all the change in the diamagnetic term. Also by symmetry, all the paramagnetic contributions in a linear system are in the perpendicular component of the shielding tensor, so

$$(2/3)\sigma_{\perp}^{\text{para}} = \sigma^{\text{para}}. \tag{14b}$$

In Fig. 4, we show only the isotropic values σ^{diam} and σ^{para} relative to the free argon atom. As expected, $[\sigma^{\text{diam}}(R) - \sigma(\infty)]$ is a monotonic function of distance, going from the value $[\sigma(\text{free Kr}) - \sigma(\text{free Ar})]$ which is 2322 ppm, down to zero at the separated atom limit. At large R, Flygare's approximation gives $[\sigma^{\text{diam}}(R) - \sigma(\infty)] = (e^2/3mc^2)18/R = 169\ (1\ \text{Å}/R)$ ppm, which, as seen in Fig. 4, is a reasonably good description of the *ab initio* σ^{diam}. As expected, σ^{para} is zero at both spherically symmetric united atom and separated atom limits, but goes negative in between.

A system that appears to have the (b) type behavior in the region of interest is the hydrogen molecule dimer $(H_2)_2$ in parallel configuration.[11] However, in the other cases reported in the literature, the positive shielding at long range might be entirely an artifact of gauge origin problems. To illustrate this, we also carried out common origin conventional CHF calculations for ^{39}Ar in the Ar_2 system. The results are shown in Fig. 5. The common origin CHF calcu-

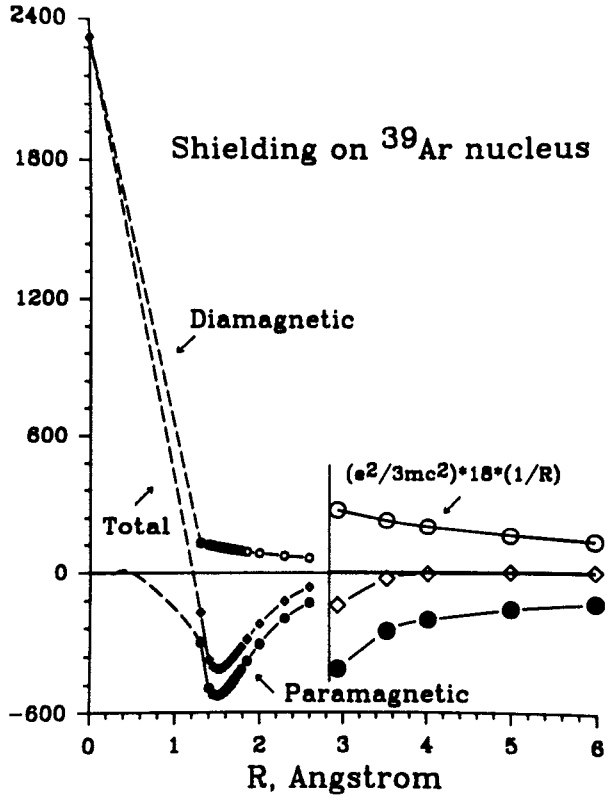

FIG. 4. *Ab initio* results for the ^{39}Ar chemical shielding in a pair of interacting argon atoms; the diamagnetic and paramagnetic parts have been determined separately for a particular choice of gauge origin—at the ^{39}Ar nucleus in question. To avoid clutter, not all the points calculated and shown in Fig. 2 are plotted here. The Flygare approximation for the diamagnetic term is shown to pass very close to the *ab initio* points at long range.

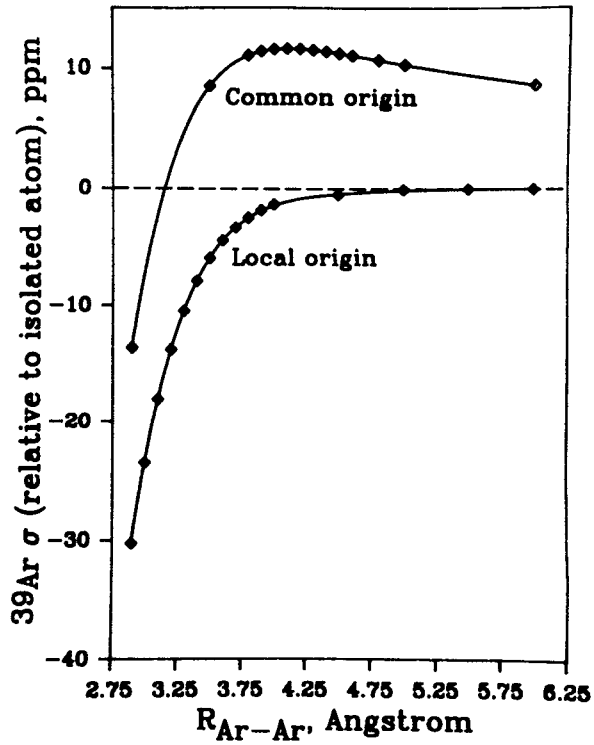

FIG. 5. The gauge origin problem is illustrated by this calculation of ^{39}Ar shielding in Ar–Ar using a conventional (common origin fixed at ^{39}Ar nucleus) CHF method. The rise and fall in shielding as the Ar atoms approach each other is an artifact.

lations underestimate the paramagnetic term, yielding a positive intermolecular shielding at large R through the entire range of internuclear separations of interest, down to $R = 3.1$ Å. As we shall see in Sec. IV, this is an unphysical result, contrary to the nearly universally observed negative medium effects on shielding of rare gas atoms. We have found that including the second-order electron correlation contributions (SOPPA) does not eliminate the positive shielding at large R when a common origin is used. The difference between these and the corresponding local origin calculations (LORG and SOLO) again proves the advantage of the latter in damping out errors due to incomplete cancellation of long-range contributions. It is evident that such errors in conventional (common origin) CHF calculations could lead to qualitatively incorrect conclusions as to the nature of the intermolecular effect on shielding. For example, whereas the conventional CHF calculations for $(CH_4)_2$ showed positive shielding at large separations,[8] the GIAO calculations showed only negative shielding at intermediate and large internuclear separations.[9] On the basis of the comparison between our Ar_2 shielding calculations using local origins (LORG and SOLO) shown in Fig. 2 and the conventional (common origin) CHF results shown here (Fig. 5), we believe that the reported positive intermolecular shieldings for $(CH_4)_2$ and for CH_4–He[8] are artifacts of the gauge origin problem. In another example, the reported positive intermolecular shieldings calculated for both ^{1}H and He in the H_2–He system[7] may also be due largely to gauge origin problems. Both ^{1}H and He shieldings calculated using a common gauge origin in the H_2–He system[7] are positive for all orientations for $R > 3.5a_0$, whereas the local origin (IGLO) shielding calculations in the related $(H_2)_2$ system[11] give very small positive values at large R and have already become negative at $R = 5a_0$.

IV. THE SECOND VIRIAL COEFFICIENT OF THE NMR CHEMICAL SHIFT IN THE GAS PHASE

We now determine whether our *ab initio* intermolecular shielding function can provide the observed behavior of the chemical shift as a function of density and temperature in the gas phase. According to Buckingham and Pople, we may expand a molecular electronic property such as shielding in a virial expansion in powers of density ρ in a gas[43]

$$\sigma(T,\rho) = \sigma_0(T) + \sigma_1(T)\rho + \sigma_2(T)\rho^2 + \cdots . \quad (15)$$

For a rare gas atom, $\sigma_0(T)$ is independent of temperature for the temperatures accessible in a NMR spectrometer, since only electronic states can contribute to internal energy in atoms and these are rather high energies. The next term is the linear dependence of the chemical shielding on the density of the gas. Buckingham gives the second virial coefficient of shielding as[20,43]

$$\sigma_1(T) = \int_0^\infty 4\pi R^2 dR\,[\sigma(R) - \sigma(\infty)] \times \exp[-V(R)/kT]. \quad (16)$$

Using the *ab initio* $\sigma(R)$ for ^{39}Ar in Ar_2, and the Ar_2 potential function $V(R)$,[38] we can calculate the second virial coefficient of ^{39}Ar chemical shielding in argon gas. These integrals are shown in Fig. 6. The sign of σ_1 calculated here is the same as has been observed for ^{129}Xe as well as other nuclei.[16] On the other hand, the artifact in the common origin results shown in Fig. 5 would have led to positive values of σ_1 at most temperatures. The shape of $\sigma_1(T)$ is qualitatively similar to what has been observed experimentally. Most of the experimental values of $\sigma_1(T)$, for various nuclei such as ^{19}F and ^{31}P and nearly all of ^{129}Xe in xenon interacting with various molecules, show the same behavior with respect to temperature as that which is exhibited by the theoretical curve for ^{39}Ar in argon gas in the left half of Fig. 6. For comparison, we show typical examples of the experimental data for ^{129}Xe in gases[44,45] in Fig. 7. On the other hand, two exceptional cases—those of ^{129}Xe in N_2 gas and ^{129}Xe in CO gas[45]—show the same behavior exhibited by the theoretical $\sigma_1(T)$ for ^{39}Ar at the higher temperatures, i.e., at temperatures about three times the well depth of $V(R)$ or higher, shown by the right half of Fig. 6. It is to be expected from Fig. 6 that if the range of temperatures at which data could be collected were to include very high temperatures, the turnabout in the magnitude of $\sigma_1(T)$ with increasing temperature could be observed in every case.

We now explore the relationship, if any, between the Drude model and the shielding function. First, we determine whether the R dependence of the intermolecular $\sigma(R)$ in the region of interest is anything like the R^{-6} of the Drude model. In Fig. 8, we examine the portion of the $\sigma(R)$ function of ^{39}Ar in Ar_2 from 2 to 3.5 Å. Figure 8 indicates that the *ab initio* $\sigma(R)$ does not have exactly an R^{-6} depend-

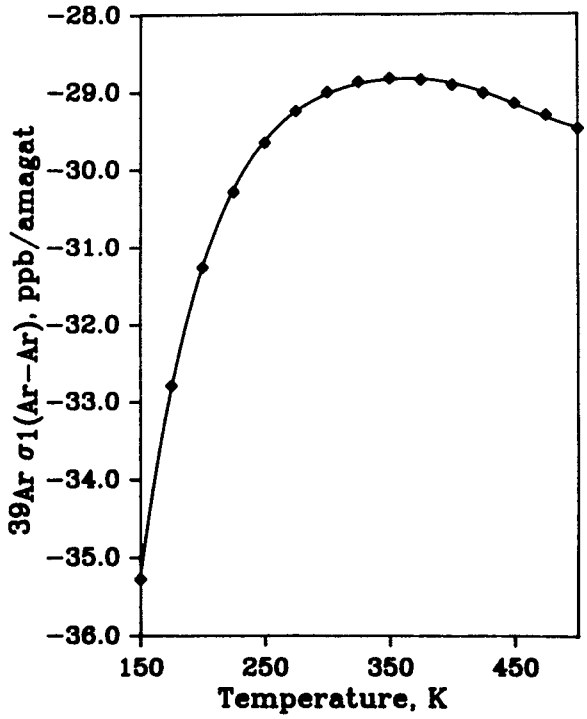

FIG. 6. The density coefficient of the chemical shielding $\sigma_1(T)$ calculated for ^{39}Ar in argon gas using the *ab initio* shielding function and Eq. (16).

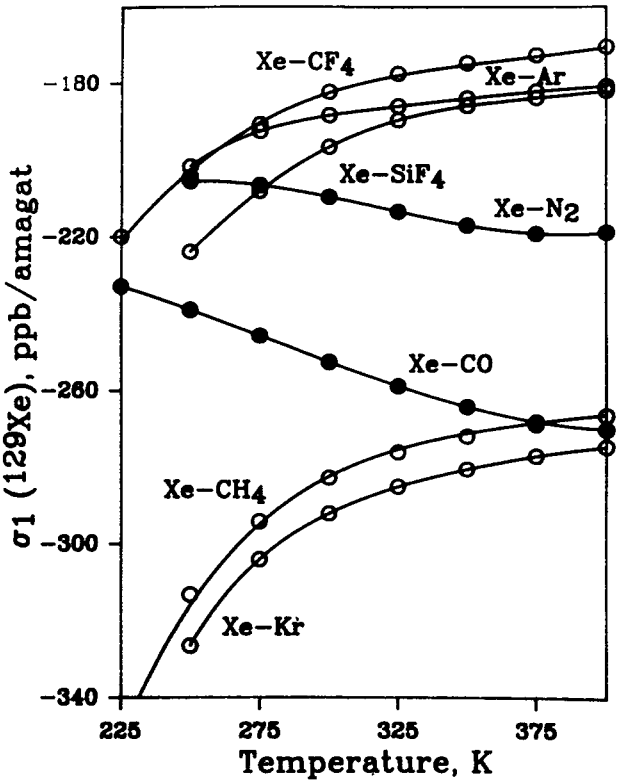

FIG. 7. Typical temperature dependence of the density coefficients of the chemical shielding measured experimentally for ^{129}Xe in various gases (data points were taken from Refs. 44–46). The temperature dependence of this quantity for ^{129}Xe in N_2 and CO gases are exceptional.

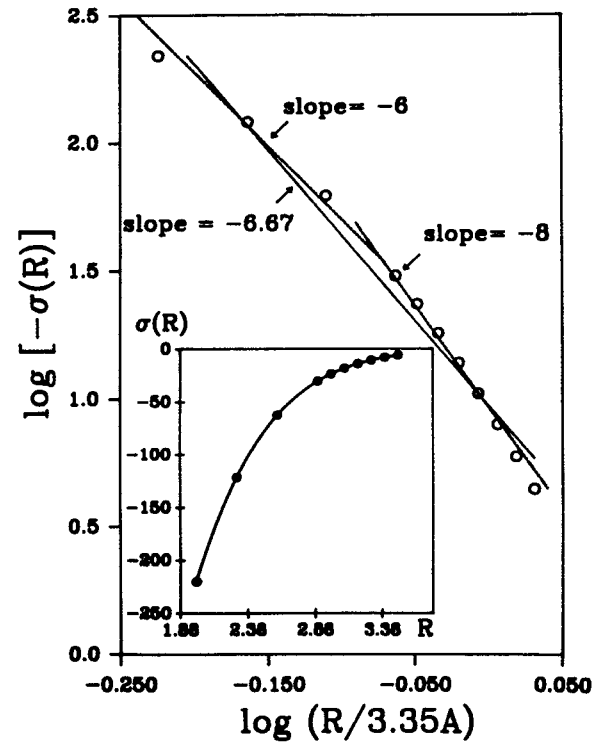

FIG. 8. The R dependence of the ^{39}Ar intermolecular shielding function relative to the free Ar atom is close to the R^{-6} form of the leading term in the Drude model.

ence; the least-squares exponent is -6.7. However, the R^{-6} behavior at 2–2.5 Å, when extended to the larger R values, gives only small absolute deviations from the *ab initio* shielding values, well within the confidence limits. Therefore, if the region of R values of interest (accessible at the temperatures in a NMR gas phase experiment) is the only regime to be considered, we find that R^{-6} is not inconsistent with the *ab initio* function. This seems to lend support to the qualitative shape of $\sigma(R)$ of the Drude model. In the Drude model for shielding, as in the dispersion energy, the R^{-6} term is only the leading term; there are R^{-8} and R^{-10} terms as well. Let us now examine the rest of the model.

The possible scaling of the $\sigma(R)$ function in the ^{39}Ar model to ^{129}Xe in Xe–Xe, Xe–Kr, and Xe–Ar shielding functions is suggested by the form of the Drude model. From Eq. (10), which is the Drude model expression for the shielding at the nucleus in atom 1 due to intermolecular interactions by atom 2, we see that the factors $B_1\alpha_2(0)U_1U_2/(U_1+U_2)$ appear as the parameters that determine the magnitude of the intermolecular chemical shift. According to the Raynes, Buckingham, and Bernstein model[20] of intermolecular effects on shielding, based on the Drude model, the parameter B is the shielding hyperpolarizability, i.e., the same B as in the shielding change in an atom due to a static external electric field F applied to the atom in Eq. (8).[24] B is therefore given by

$$B=\tfrac{1}{6}[(\partial^2\sigma_\parallel/\partial F^2)_{F=0}+2(\partial^2\sigma_\perp/\partial F^2)_{F=0}], \quad (17)$$

where $\sigma_\parallel$ and $\sigma_\perp$ are the shielding tensor components parallel and perpendicular to the applied electric field. Therefore, the value of B in this model is a property only of the rare gas atom carrying the NMR nucleus. It is well known that the magnitudes of NMR chemical shifts of nuclei across the Periodic Table scale as $\langle a_0^3/r^3\rangle$ for the valence p electrons of the atom in question, a quantity which can be derived directly from the spin–orbit splittings observed in atomic spectra. In other words, the sensitivity of the nuclear shielding to changes in the electronic environment of the nucleus (e.g., in going from one molecule to another) has been found to be reflected by $\langle a_0^3/r^3\rangle$ for the free atom.[46] Thus, we may expect the shielding hyperpolarizability to scale as $\langle a_0^3/r^3\rangle$. The distortion of the electron distribution in an atom upon being placed in a static electric field depends on the static electric dipole polarizability of the atom. Therefore we suggest that B scales as the product $\alpha(0)\langle a_0^3/r^3\rangle$, reflecting both the degree to which the electron distribution is modified and the sensitivity of the nuclear shielding to that modification. Summarizing, we suggest that in the region of interest $[\sigma(R)-\sigma(\infty)]$ for any rare gas pair can be obtained by scaling the *ab initio* function $[\sigma(R)-\sigma(\infty)]$ calculated for ^{39}Ar in Ar_2 by the factor $\alpha_1(0)\langle a_0^3/r^3\rangle_1\,\alpha_2(0)U_1U_2/(U_1+U_2)$, where B_1 is assumed to scale as $\alpha_1(0)\langle a_0^3/r^3\rangle_1$. Furthermore, since this shielding arises from intermolecular interactions, the intermolecular distances have to be scaled according to the law of corresponding states for interacting molecules, i.e., in each case R is scaled according to respective intermolecular potential functions. For this purpose, the potential functions scaled to Ar–Ar in Maitland *et al.* (their Table A3.2) are ideal and these

have been used here.[38] Thus, the ^{39}Ar intermolecular shielding function in Fig. 2 was scaled up to ^{129}Xe in the Xe–Xe, Xe–Kr, and Xe–Ar interacting pairs, as in the following example:

$$[\sigma(R/r_0)-\sigma(\infty)]_{^{129}\text{Xe in Xe-Kr}} = \frac{2\alpha_{\text{Xe}}(0)\langle a_0^3/r^3\rangle_{\text{Xe}}\alpha_{\text{Kr}}(0)U_{\text{Xe}}U_{\text{Kr}}}{\alpha_{\text{Ar}}(0)\langle a_0^3/r^3\rangle_{\text{Ar}}\alpha_{\text{Ar}}(0)U_{\text{Ar}}(U_{\text{Xe}}+U_{\text{Kr}})} \times[\sigma(R/r_0)-\sigma(\infty)]_{^{39}\text{Ar in Ar-Ar}}. \quad (18)$$

With these ^{129}Xe intermolecular shielding functions, we can then perform the integration in Eq. (16) to obtain the appropriate $\sigma_1(T)$, using the $V(R)$ functions for Xe–Ar, Xe–Kr, and Xe–Xe from the compilation in Maitland *et al.*[38] The results are shown in Fig. 9, where they are compared with the experimental values.[47,48] The calculated $\sigma_1(T)$ values reproduce the order of magnitudes of the experimental data quite well, have the correct sign of the temperature dependence, and reproduce the relative changes observed in going from the Xe–Ar to Xe–Kr to Xe–Xe systems. It appears that the scaling factors that we have found do reflect the variation in the intermolecular shielding function in rare gas systems for the range of distances where the Drude model might be expected to be roughly valid. It is important to note that no adjustable parameters have been used here. The scaling factor contains only independently measured experimental quantities. Of course, this scaling is not expected to apply to the very short-range regions of $\sigma(R)$. It is not yet clear what factors influence the magnitude of the shielding at the minimum of the shielding function, or the intermolecular distance at which the minimum is located. Neither the separation at which the minimum occurs nor the value of the shielding at the minimum have been observed previously in *ab initio* calculations. The very short-range regions of $\sigma(R)$ can be explored with NMR experiments at ultrahigh pressures.

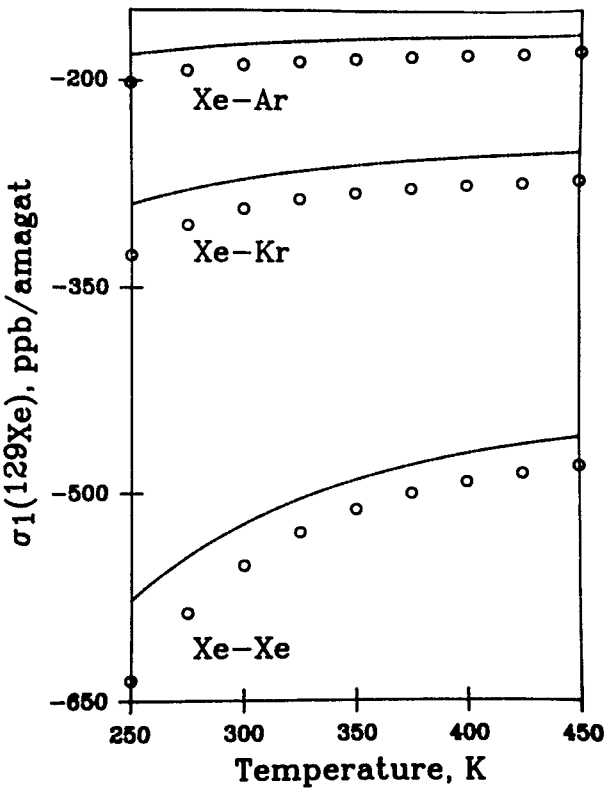

FIG. 9. The curves are thermal averages $\sigma_1(T)$ obtained from Eq. (16) by using the intermolecular shielding functions $\sigma(R)$ for ^{39}Ar in Ar–Ar scaled to $\sigma(R)$ for ^{129}Xe in Xe–X. The points are the experimental data from Refs. 47 and 48.

The successful scaling of the *ab initio* ^{39}Ar shielding to provide ^{129}Xe chemical shifts in the gas phase prompts us to extend the method to the observed gas-to-solution chemical shifts for rare gases. Williamson and co-workers have measured large gas-to-solution shifts for ^{129}Xe in a variety of organic solvents.[49] Subsequently, the ^{83}Kr gas-to-solution shifts were measured and compared to the ^{129}Xe shifts.[50] Recently, Diehl *et al.* have measured ^{21}Ne gas-to-solution shifts in the same set of organic solvents as were used for ^{129}Xe and ^{83}Kr.[51] The corresponding ^{83}Kr and ^{129}Xe shifts in the same solvent form a straight line. The corresponding ^{21}Ne and ^{129}Xe shifts in the same solvent likewise form a straight line. The range of gas-to-solution shifts is 12.5 ppm for ^{21}Ne, 140 ppm for ^{83}Kr, and 250 ppm for ^{129}Xe. We interpret these gas-to-solution chemical shifts by using the scaling method described above. Consider the liquid solvent to provide a cavity for the dissolved rare gas atom. Using the same approach as London, we equate the dispersion energy to

$$W_{\text{dispersion}} \approx -\tfrac{3}{2}\alpha_1(0)U_1 g(\epsilon,a)U_2/(U_1+U_2), \quad (19)$$

where we envision a dissolved rare gas atom in a cavity of radius a in the liquid solvent of dielectric constant ϵ. This expression is the same as that used by Howard *et al.*[52] $g(\epsilon,a)$ is a function of the properties of the liquid solvent. The mean-square effective static electric field at the rare gas nucleus due to the mutual interaction of the rare gas atom and the dielectric medium is

$$\overline{F_{\text{eff}}^2} \approx \tfrac{3}{2}U_1 g(\epsilon,a)U_2/(U_1+U_2). \quad (20)$$

Accordingly, the shielding associated with the response to this mean-square field is $-B_1\,\overline{F_{\text{eff}}^2}$. The free-atom-to-solution shift for rare gas atom 1 is

$$\delta \approx B_1 \tfrac{3}{2} g(\epsilon,a)U_1U_2/(U_1+U_2). \quad (21)$$

Neglecting the small shift from the free atom to the low density gas, the range of gas-to-solution shifts for a given rare gas atom 1 is

$$\delta''-\delta' \approx B_1 \frac{3}{2} U_1 \left\{\frac{g''(\epsilon,a)U_2''}{(U_1+U_2'')} - \frac{g'(\epsilon,a)U_2'}{(U_1+U_2')}\right\}. \quad (22)$$

For the same set of extreme solvents ($'$ and $''$) and assuming U_1 differences to be not too large that we may use an average U_1 within the curly brackets, we should find that the range of gas-to-solution shifts of a rare gas atom in the same set of solvents to be proportional to the product of the shielding hyperpolarizability B and the ionization potential U of the rare gas atom. As we have already seen that B scales as the

product $\langle a_0^3/r^3\rangle\alpha(0)$, we expect the range of the gas-to-solution shifts to be proportional to $\langle a_0^3/r^3\rangle\alpha(0)U$ of the rare gas atom. We show this in Fig. 10, where we have used the experimental data from the three laboratories.[49–51] The reasonably good straight line passing through the origin attests to the success of our scaling scheme. A straight line plot of these gas-to-solution shift data against σ (free atom) had been used to support the hypothesis that the gas-to-solution shift comes nearly entirely from the diamagnetic term in shielding.[51] This hypothesis does not appear to be correct, based on the *ab initio* calculations shown in Fig. 4. On the other hand, the correlation of σ(free atom) with $\langle a_0^3/r^3\rangle\alpha(0)U$ is not entirely surprising. Assumption of a mean excitation energy and closure gives $\alpha(0) \approx (2/3)e^2\langle r^2\rangle/U$, whereas σ(free atom) $= (e^2/3mc^2)\langle 1/r\rangle$.

A further check on the scaling factors for the intermediate distances is provided by comparison of two *ab initio* shielding functions. For this purpose, we have carried out a calculation of the ^{21}Ne shielding as a function of the intermolecular distance in Ne_2. The results are shown in Fig. 11. The minimum shielding for ^{21}Ne is -167.51 ppm at 1.00 Å, to be compared with -413.64 ppm at 1.50 Å for ^{39}Ar in Ar_2. It is not surprising that the shieldings at very short range do not scale when using the factors based on the Drude model $\alpha_1(0)\langle a_0^3/r^3\rangle_1\alpha_2(0)U_1U_2/(U_1+U_2)$. However, the *ab initio* ^{21}Ne and the scaled ^{39}Ar shieldings in the intermediate range of distances can be compared. In Fig. 11, the *ab initio* shielding for ^{39}Ar in Ar_2 has been scaled down to ^{21}Ne in Ne_2, giving the predicted ^{21}Ne shielding function shown by the solid curve from 2.25 to 3.50 Å. This is seen to reproduce reasonably well the *ab initio* calculated shielding values for ^{21}Ne in Ne_2 given by the points shown. The near correspondence of the two gives us some indication that in the R region of interest, our suggested scaling factor has some validity.

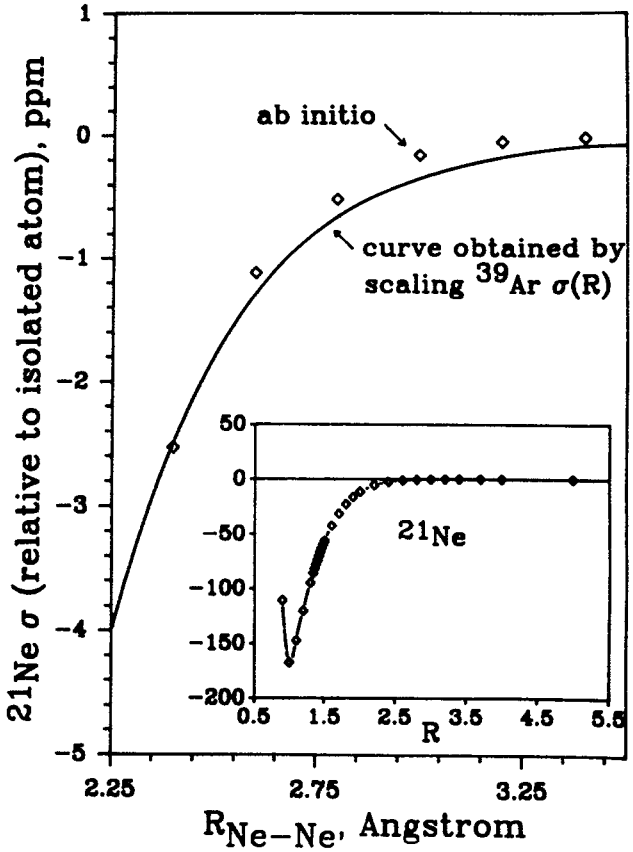

FIG. 11. The points are the *ab initio* intermolecular shielding values for ^{21}Ne in Ne interacting with another Ne atom. In the intermediate and long R values, ^{39}Ar in the Ar–Ar *ab initio* shielding function has been scaled down to ^{21}Ne in Ne–Ne (solid curve) for comparison.

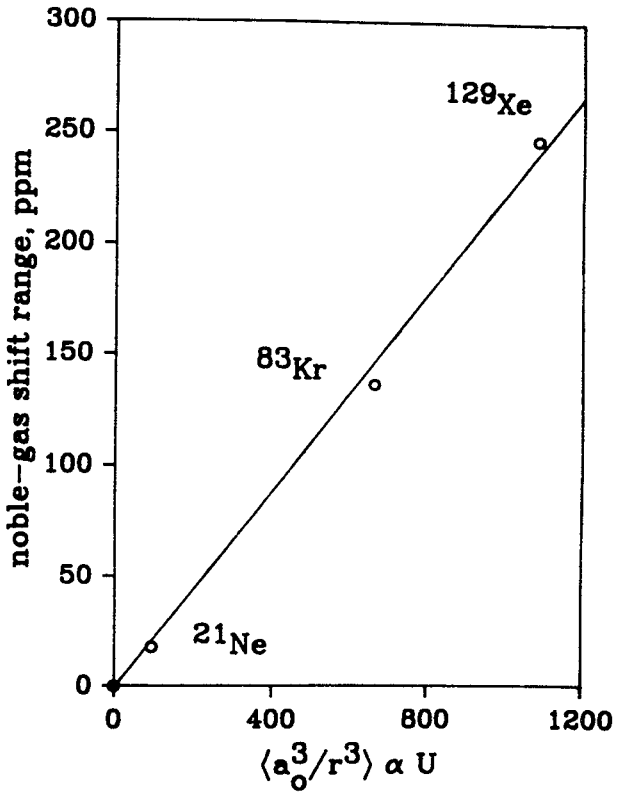

FIG. 10. The ranges of gas-to-solution chemical shifts for neon, krypton, and xenon measured in a common set of organic liquids (Refs. 49–51) are compared against the scaling factors we have used here.

V. COMPARISON OF THE INTERMOLECULAR AND INTRAMOLECULAR SHIELDING FUNCTIONS

An interesting comparison can be made with the intramolecular shielding function $\sigma(R)$ calculated by Hegstrom[5] for the simplest diatomic molecule H_2^+ and the intramolecular potential function $V(R)$ for this molecule shown in Fig. 12. Many other calculations of the intramolecular shielding function show the same behavior in the vicinity of R_e; i.e., it is found commonly for diatomic molecules (and also for polyatomic molecules) that $(\partial\sigma/\partial R)_e < 0$.[53] This is probably a typical shape of the intramolecular $\sigma(R)$ in diatomics, although the shielding value at the equilibrium separation can be less than the diamagnetic shielding in the separated

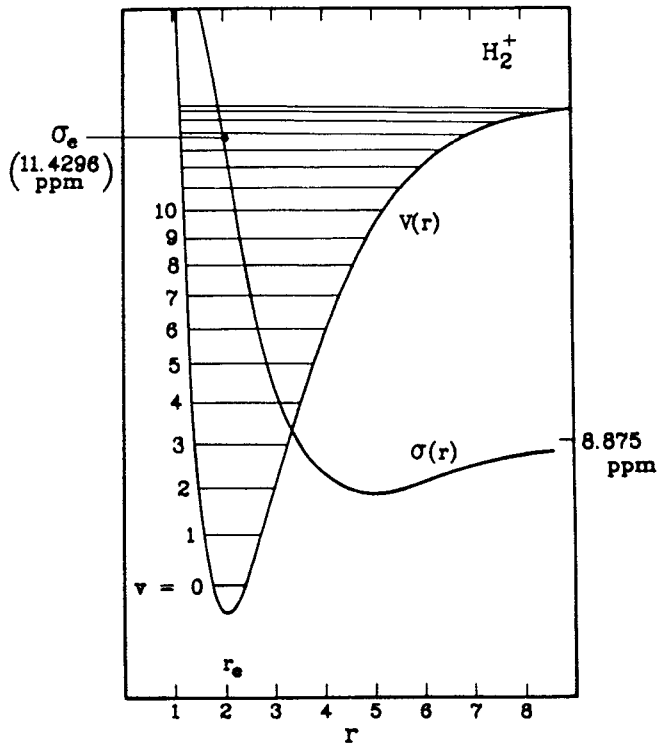

FIG. 12. The ^{1}H chemical shielding in the H_2^+ molecule from very accurate calculations by Hegstrom (Ref. 5). The H_2^+ intramolecular potential function is also shown. Reproduced from Ref. 53, with permission.

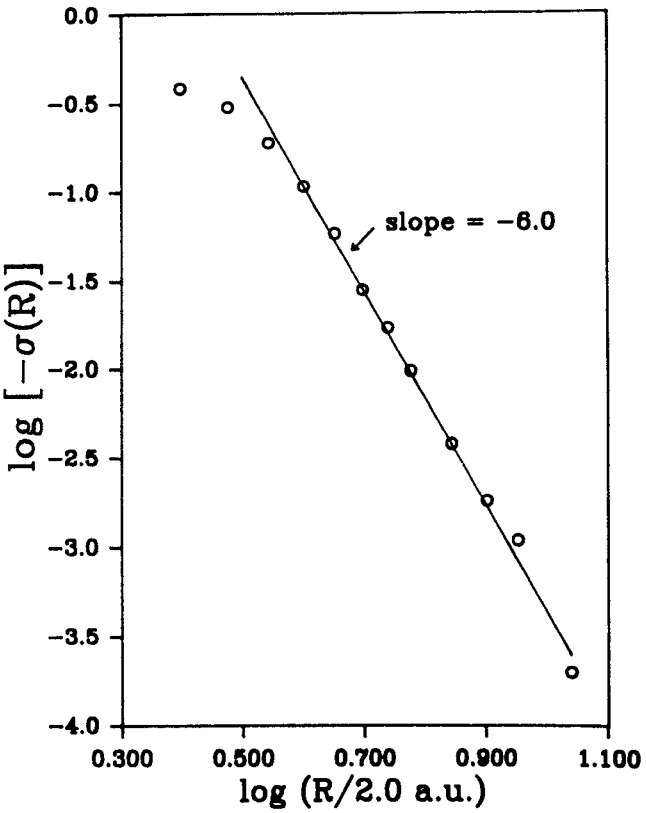

FIG. 13. The R dependence of the ^{1}H shielding function $[\sigma(R) - \sigma(\infty)]$ in the H_2^+ molecule for R values beyond the shielding minimum ($R = 4.5$–22.0 a.u) is very close to R^{-6}.

atom, as for the ^{19}F nucleus in the F_2 molecule.[54] (There are examples of qualitatively different behavior in the shielding functions of electropositive elements, however.[55]) It is probably typical that the internuclear separation corresponding to the minimum shielding is well inside the equilibrium internuclear separation for the *inter*molecular shielding, but is outside of the equilibrium internuclear separation for the *intra*molecular shielding.

Let us now consider the *inter-* and *intra*molecular shielding from a unified point of view. Both shielding functions have the same general qualitative shape, exhibiting a minimum at some separation. Furthermore, the behavior of the shielding functions at large R can be compared. In Fig. 13, we exhibit the nearly R^{-6} dependence found in the *intra*molecular shielding function $[\sigma(R) - \sigma(\infty)]$ for ^{1}H in the H_2^+ molecule in that section of the function corresponding to distances greater than the shielding minimum. Comparing Figs. 8 and 13, it is interesting that both the *inter*molecular shielding function for ^{39}Ar in the van der Waals molecule Ar_2 and the *intra*molecular shielding function for ^{1}H in the H_2^+ molecule behave roughly as R^{-6} at separations longer than the separation corresponding to the shielding minimum. The main difference comes about in the sampling over the range of R values. In covalent diatomic molecules, the *intra*molecular potential minimum occurs at shorter distances than the shielding minimum, whereas in diatomic van der Waals molecules, the *inter*molecular potential minimum occurs at separations larger than the shielding minimum.

How universal is the shape of the shielding function? For *inter*molecular shielding, we have found that in the range of intermolecular distances sampled by $\exp[-V(R)/kT]$ at ~ 300 K, the functional form of the *ab initio* $\sigma(R)$ for ^{39}Ar in Ar_2 is sufficiently representative of the form for any two rare gases so that scaling factors convert the Ar_2 function in this region to reproduce quantitatively experimental data for ^{129}Xe in Xe–Ar, Xe–Kr, and Xe–Xe in the gas phase, and also reproduce quantitatively the *ab initio* ^{21}Ne shielding function in Ne_2 in the interesting region. The success in the choice of the scaling factor lies in correctly attributing the change in shielding to the relevant type of interaction and to the relevant regime of coordinates. For the interacting rare gas atoms, the shielding change is due to the induced dipole–induced dipole interaction. In the regime of coordinates sampled by the factor $\exp[-V(R)/kT]$, the $\sigma(R)$ values scale according to the factors discovered upon consideration of the Drude model, which provides a physical mechanism for the shielding at intermediate and long range. At the very short range, where overlap of orbitals is a maximum and shielding is minimum, the intermolecular $[\sigma(R) - \sigma(\infty)]$ does not scale.

For *intra*molecular shielding, the analogous region of interest is that sampled during molecular vibration, i.e., in the vicinity of R_e. The equilibrium geometry contains in itself the nature of the interaction, covalent bonds that result

from a positive overlap of orbitals. For the intramolecular shielding function, it is the magnitude of the shielding change relative to its value at the minimum energy geometry which is of interest. We have found previously that in the vicinity of the equilibrium molecular geometry, the intramolecular shielding functions ($\sigma - \sigma_e$) for ^{31}P in the PH_3 molecule and the ^{15}N nucleus in the NH_3 molecule scale according to $\langle a_0^3/r^3 \rangle$ of the P and N atoms.[33] When scaled according to $\langle a_0^3/r^3 \rangle$, the traces on the multidimensional shielding surface that describe the variation of the ^{31}P and ^{15}N shieldings with respect to each of the symmetry-related nuclear displacement coordinates $S_1 = 3^{-1/2}(\Delta r_1 + \Delta r_2 + \Delta r_3)$, $S_3 = 6^{-1/2}(2\Delta r_1 - \Delta r_2 - \Delta r_3)$ (two of these), and $S_4 = 6^{-1/2} r_e (2\Delta r_1 - \Delta r_2 - \Delta r_3)$ (two of these) are found to be nearly superposable for all values of the displacement coordinates sampled during ordinary vibrations. Far removed from these geometries, the ^{31}P and ^{15}N shielding functions diverge. For these analogous molecules, only the shielding changes with respect to opening and closing up of the bond angles (the umbrella or inversion motion described by the S_2 coordinate) do not superpose. Although we sometimes find $\langle a_0^3/r^3 \rangle$ scaling of the shielding in a molecule in the vicinity of the equilibrium geometry, this may not be the dominant factor in every case; we present this merely for the sake of comparison. In going from one molecule to another, the sensitivity of the shielding expressed by $\langle a_0^3/r^3 \rangle$ is not necessarily the dominating factor in the shape of the shielding function in the vicinity of the equilibrium geometry. While we have uncovered several factors that enter into the scaling of the intermolecular shielding, we have so far merely tested the $\langle a_0^3/r^3 \rangle$ factor in the intramolecular system in a case where, fortuitously, all other factors may be compensating each other.

In summary, we find that a unified view of the shielding function in van der Waals systems (intermolecular) and in diatomic molecules (intramolecular) is possible. The shielding property is electronic in origin and the change in this property originates from a perturbation of the electronic distribution around the nucleus. It is therefore not surprising to see shielding functions so intimately related to the potential functions. That the shielding functions lend themselves to a scaling procedure using scaling factors dependent on the type of interaction dominant in that region of interest indicates that there are some universal features of these functions and offers hope of using *ab initio* calculations on small systems to interpret observations made in larger systems.

VI. THE NMR CHEMICAL SHIFT OF ADSORPTION

The sensitivity of the chemical shielding to the environment of the molecule having been established in the gas phase, the ^{129}Xe NMR chemical shielding offers the possibility of reporting on molecule–surface interactions, especially in porous materials with internal surfaces and molecular size cages. The advantages offered by xenon in gas phase studies are even more evident here. The very large chemical shift range guarantees that the adsorbed xenon signals can be definitely resolved from the free xenon signals. The bulk susceptibility of the sample leads to a shift of the NMR signal by about 1–2 ppm even in the complete absence of any interaction. This shift is the same for any observed nucleus in the sample. While this bulk effect would dominate the shift of a proton signal, making it difficult to extract the shift due to interactions with the surface, this bulk susceptibility shift is negligible compared to the ^{129}Xe chemical shift range of the xenon atom in various environments. The size of the xenon atom is about right; it can enter pores which are accessible to the CH_4 molecule. Thus, the pores in which any interesting chemistry can take place can be explored by xenon atoms. These advantages have made the ^{129}Xe NMR chemical shift a widely used probe of microporous solids such as zeolites, clays, coals, etc.[3,56,57] It is found that the ^{129}Xe chemical shift in zeolites and its change with xenon loading can be used as a signature of the zeolite type, the major factor being the sizes of the cavities within the crystallites.[3] The ^{129}Xe chemical shift has also been used to detect the presence and distribution of other guest molecules inside the cavities.[58–60] In these studies, a single Xe signal is observed, which is an average over all the environments visited by the diffusing xenon atoms within the NMR time scale. A very important component of the interpretation of these types of data is a modeling of the distribution and the dynamics of the xenon atom within the pores of the zeolites, in addition to an understanding of the chemical shift due to interaction within one cavity.

We have observed ^{129}Xe NMR spectra of xenon atoms trapped in identical cages, such that at room temperature, the xenon atoms have negligible cage-to-cage motion during the NMR experiment.[14] Therefore, we are able to see the resolved signals from individual cages occupied by only one Xe atom or two or more, up to eight Xe atoms. These observations of ^{129}Xe chemical shifts in dehydrated zeolite NaA can be interpreted with the help of the *ab initio* calculations presented here. The alpha cage in which the xenon atoms are trapped is shown in Fig. 14. This schematic diagram of a

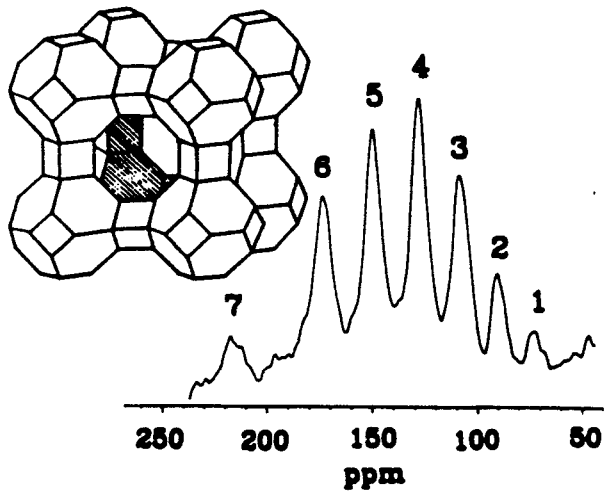

FIG. 14. The ^{129}Xe NMR spectrum of xenon atoms adsorbed in zeolite NaA; the chemical shifts are in ppm relative to a free xenon atom. The structure of zeolite A is described schematically by lines representing a T–O–T unit, where T is either Si or Al in the formula $[(AlO_2)_{12}(SiO_2)_{12}]^{12-}$.

pseudounit cell of zeolite NaA represents a T–O–T unit (T = Si or Al) as a straight line. The Na^+ ions are located at the centers of the six oxygen rings (shown as hexagons in the diagram). There are eight such Na^+ ions. One more ion is in a special location very close to a four ring. The remaining three ions are the six Na^+ ions located in the plane (not quite at the centers) of the windows to the alpha cage, each shared with a neighboring cage.[61] A typical ^{129}Xe NMR spectrum of xenon atoms trapped in these alpha cages is shown in Fig. 14. The observed peaks are due to those alpha cages containing, respectively, one, two, three, ..., seven trapped xenon atoms. At higher xenon loadings of the zeolite, eight xenon atoms have also been observed by us.[14] The ^{129}Xe chemical shift of the single Xe atom in a cage is 74.8 ppm relative to a free xenon atom. At 300 K, the increments upon adding one more Xe atom to the cage are close to 20 ppm for Xe_2 up to Xe_6, increasing slightly as follows: 17.5, 19.4, 21.5, 25.2, 25.1 ppm, i.e., at 300 K,

$$\sigma(\text{Xe in } \alpha \text{ cage}) - \sigma(\text{free atom}) = -74.8 \text{ ppm},$$
$$\sigma(\text{Xe}_2 \text{ in } \alpha \text{ cage}) - \sigma(\text{Xe in } \alpha \text{ cage}) = -17.5 \text{ ppm},$$
$$\sigma(\text{Xe}_3 \text{ in } \alpha \text{ cage}) - \sigma(\text{Xe}_2 \text{ in } \alpha \text{ cage}) = -19.4 \text{ ppm},$$

etc. Beyond six xenon atoms, there is a dramatic change; large changes in the chemical shift increment from Xe_6 to Xe_7 (45.1 ppm) and from Xe_7 to Xe_8 (43.7 ppm) are observed. Each of the peaks has a temperature dependence which we also measured.[14]

One of the important questions raised in empirical NMR studies of ^{129}Xe in xenon atoms trapped in zeolites is "how important are the contributions to the ^{129}Xe chemical shift due to the interactions of the xenon atoms with the counterions present in the zeolite?" The ions are certainly important in the interaction energy; nearly all the approximate potential energy surfaces determined for CH_4 or Xe in zeolites *A* or the faujasites show minima near the counterion sites.[62–66] As our contribution to the understanding of the NMR chemical shift observed in adsorption studies, we present here some *ab initio* calculations with the following goals: (a) to estimate the effect of the counterion, to determine the sign and magnitude of the ^{129}Xe shifts upon interaction with the Na^+ ions in the cavity, and to estimate how important these are compared to Xe–O and Xe–Xe interactions; (b) to understand the sign and magnitude of the chemical shift of a single Xe atom in a cavity relative to a free Xe atom; (c) to understand the direction of the chemical shift due to the second Xe atom in the cavity; (d) to understand the near additivity and the slight increase of increments in the ^{129}Xe chemical shift with an increasing number of xenon atoms for Xe through Xe_6 in the cavity; (e) to understand the large increment in chemical shift between Xe_7 and Xe_6 and between Xe_8 and Xe_7; and (f) to understand the temperature dependence of each of the eight chemical shifts.

To help elucidate the role of counterions in chemical shifts, we carried out calculations of the ^{39}Ar shielding (as a model for ^{129}Xe) in the Ar atom interacting with the Na^+ ion over the same wide range of intermolecular distances as we have used for the calculations on an Ar atom interacting with another Ar atom. Figure 15 shows the results. There are several points worth noting here. One is that whereas the contributions of second-order correlation are too small to show up on this plot for the Ar–Ar system, they are fairly substantial near the minimum shielding for Ar in the presence of the Na^+ ion. The numerical values are given in Table II. Contrary to conventional belief that electron correlation effects are more important in dispersion interaction than induction, this seems to indicate that for this molecular electronic property, electron correlation may be rather important for induction effects. Nevertheless, in the region of interest, where the two-atom potentials give significant weighting (shown in the inset in Fig. 15), the correlation

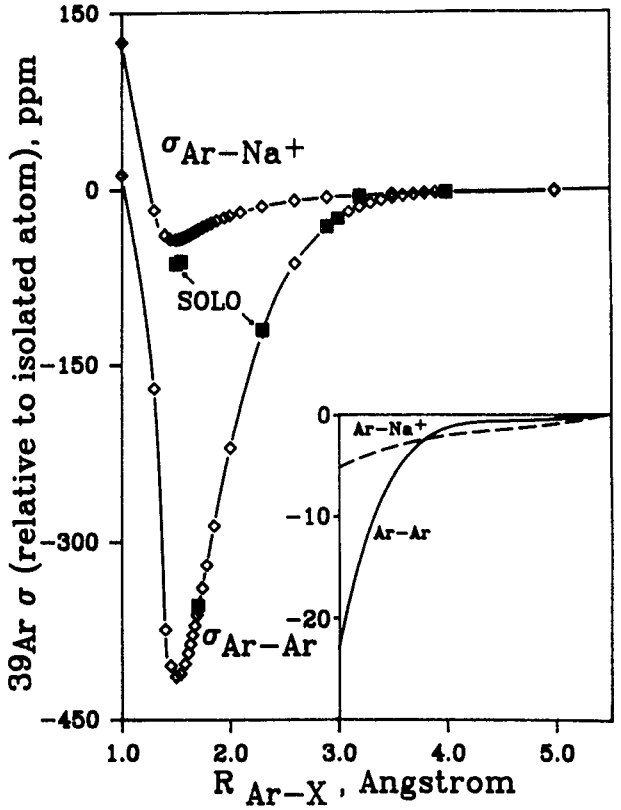

FIG. 15. The *ab initio* intermolecular shielding for ^{39}Ar in the Ar atom interacting with the Na^+ ion. The SOLO calculations include the contributions from second-order electron correlation to chemical shielding which are not present in LORG. The shielding is compared to ^{39}Ar in Ar interacting with an argon atom, where SOLO provides values which do not differ visibly from the LORG values.

TABLE II. Chemical shielding values for ^{39}Ar in an argon atom interacting with a Na^+ ion with (SOLO) and without (LORG) second-order electron correlation.

	$[\sigma(R) - \sigma(\infty)]$ (ppm)	
R (Å)	LORG	SOLO
1.50	−42.60	−62.85
1.56	−39.78	−60.78
3.20	−4.77	−5.55

contributions to the ^{39}Ar shielding are not visible. A comparison of the ^{39}Ar shielding in the Ar–Na^+ pair with the Ar–Ar pair in Fig. 15 shows that a neighboring cation has a much smaller contribution to the Ar shielding than does an Ar atom at the same distance, despite the much deeper well associated with the Ar–Na^+ potential surface than the Ar–Ar potential surface. The long-range behavior of the ^{39}Ar shielding in the interaction with a Na^+ ion is different from that in the interaction with an Ar atom. While the shielding function in the Ar–Ar system falls off as R^{-6} and R^{-8}, in the Ar–Na^+ system the shielding function falls off more slowly (see the inset in Fig. 15), closer to an R^{-4} behavior. The induction contributions may be somewhat less in the zeolite alpha cage, where the effective positive charge on Na may not be as large as in the bare Na^+ ion.

A single Xe atom in an alpha cage is surrounded by 72 oxygen atoms (of which 48 belong wholly to the cage and 24 are shared with neighboring cages) and 15 Na^+ ions (of which nine belong wholly to the cage and six are shared with neighboring cages). It is this environment which gives rise to the 74.8 ppm chemical shift between the xenon atom inside the cage and the isolated xenon atom. We cannot model this with *ab initio* calculations, but the Drude model provides a reasonable approximate result. We have noted in Sec. II that in the Drude model for two interacting atoms, there is a relationship between the intermolecular shielding $\sigma(R)$ and the London dispersion energy $W(R)$ for the system, i.e., at distances for which the Drude model is approximately valid, the shielding relative to the isolated atom is given approximately by

$$[\sigma(R)-\sigma(\infty)]\approx[B/\alpha(0)]W(R), \tag{23}$$

where $\alpha(0)$ is the static electric dipole polarizability of the atom in which the magnetic nucleus resides. In this way, we describe both $\sigma(R)$ and $W(R)$ with the same physical model. This model can also be applied to a xenon atom inside a zeolite pore. If, as Schmeits and Lucas have done, we consider the adsorption energy in terms of a model in which the zeolite alpha cage is idealized as a spherical cavity in a solid which is a continuum of dynamical dielectric function $\epsilon(\omega)$, the surface localized electronic oscillations play the essential role in the interaction between the atom and the surface. Schmeits and Lucas have derived the expressions for the atom–surface energy in terms of the atom–dynamic dipole polarizability $\alpha(\omega)$ and the solid $\epsilon(\omega)$.[67,68] Where R is the distance from the center of the cavity of radius a, the adsorption energy $W(R)$ is given by[67,68]

$$W(R)=-(\hbar/2\pi)(1/R^3)\sum_{k=1}^{\infty}k(k+1)(R/a)^{2k+1}\times\int_0^{\infty}\alpha(i\xi)\frac{\epsilon(i\xi)-1}{\epsilon(i\xi)+k/k+1}d\xi, \tag{24}$$

where $i\xi=\omega$. Derouane *et al.*[69] have summed up the geometric series in Eq. (24) for the case (such as when ϵ is very large) where the integral is independent of k. Furthermore, the integral can be approximated by $\alpha(0)\hbar\omega_0$, where $\alpha(0)$ is the static electric dipole polarizability of the atom, and the Drude oscillator frequency $\hbar\omega_0$ can be taken as its ionization potential U,

$$W(R)\approx-[\alpha(0)U/a^3][1-(R/a)^2]^{-3}. \tag{25}$$

The Drude model for the shielding of the atom in the spherical cavity, relative to the free atom, is then given by

$$[\sigma(R)-\sigma(\infty)]\approx-(BU/a^3)[1-(R/a)^2]^{-3}. \tag{26}$$

A reasonable value for the cavity radius a for zeolite A is 7.08 Å (an average center of cage to oxygen distance based on x-ray diffraction data).[70] Based on Lennard-Jones pairwise interactions integrated over a spherical cavity and Table I of Derycke *et al.*,[71] we find that the position of minimum energy for a Xe atom in a sphericalized cavity of oxygen atoms (cavity radius 7.08 Å) is $R_e=4.174$ Å. There is an old estimate of the value of B for the Xe atom, $B\approx337.3\times10^{-18}$ esu or 9.83×10^4 ppm/a.u.^{2}.[72] The first ionization potential is 0.445 76 a.u. for the Xe atom. Using these quantities, we find $[\sigma(R_e)-\sigma(\infty)]\approx-66$ ppm, to be compared with the experimental thermal average value we observed -74.8 ppm for a single Xe atom in an alpha cage of zeolite NaA at 300 K.[14] In the above model, the spherical cavity takes no account of the corrugation of the inner surface of the alpha cage. Also, the chemical shift should have been obtained by a proper average over the radial distribution function $\rho(R,T)$,

$$\delta_1\approx(BU/a^3)\int_0^a 4\pi R^2dR\,[1-(R/a)^2]^{-3}\rho(R,T) \tag{27}$$

rather than taking $\delta_1\approx(BU/a^3)[1-(R_e/a)^2]^{-3}$. The advantage of the model lies in its simplicity. Using the same value of B, it is possible with this simple model to relate the ^{129}Xe chemical shift observed (at the zero loading limit, uncontaminated by Xe–Xe interactions) in zeolites of various pore sizes with the pore size. Indeed, it has been shown by Derouane *et al.*[73,74] that a very useful linear relationship holds between δ_1 and $W(R_e)$ over a range of δ_1 values up to 250 ppm, and the straight line nearly passes through the origin. Furthermore, Eq. (25) has been used by Derouane[75] to calculate theoretical values of isosteric heats of sorption of sorbate molecules of various polarizabilities and molecular dimensions in zeolites of various pore sizes and shapes. He finds a very good correlation of the theoretical values with the experimental values.

We can model the incremental shifts upon addition of one Xe atom at a time if we make the assumption that the chemical shifts due to Xe–Xe interactions are not modified significantly by the alpha cage. If we make this assumption, then we can compare the relative ^{39}Ar chemical shifts between Ar, Ar_2, Ar_3,... clusters in field-free space with the increments in the observed ^{129}Xe chemical shifts in the Xe, Xe_2, Xe_3,... systems trapped inside the alpha cages.

For this purpose, we carried out LORG calculations for ^{39}Ar in two symmetrical trimers, the linear Ar–Ar–Ar, and the Ar_3 equilateral triangle to model the observed increments for the Xe, Xe_2, and Xe_3 clusters trapped in zeolite NaA. To save time, we only considered these symmetrical geometries. Figure 16 shows that there are incremental changes in the shielding, i.e., at any of the relevant internuclear separations, the Ar_2 shieldings are negative compared to the single Ar atom and the Ar_3 shieldings are larger nega-

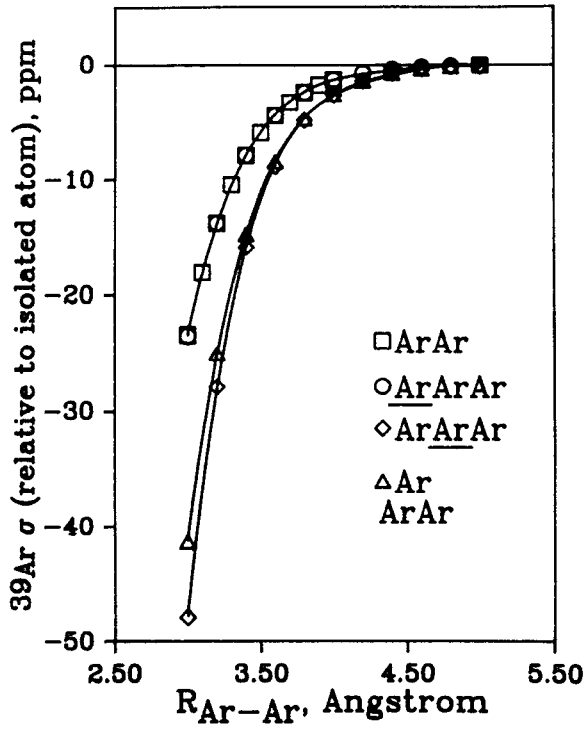

FIG. 16. A comparison of ^{39}Ar shielding in Ar, Ar_2, and Ar_3. Only the symmetrical linear and triangular configurations were considered for the Ar_3 cluster. At these intermediate distances, the shielding of the end Ar atom in the symmetrical linear Ar_3 is very similar to that for Ar_2. The linear and triangular configurations have diverging shielding values at much shorter distances than shown here.

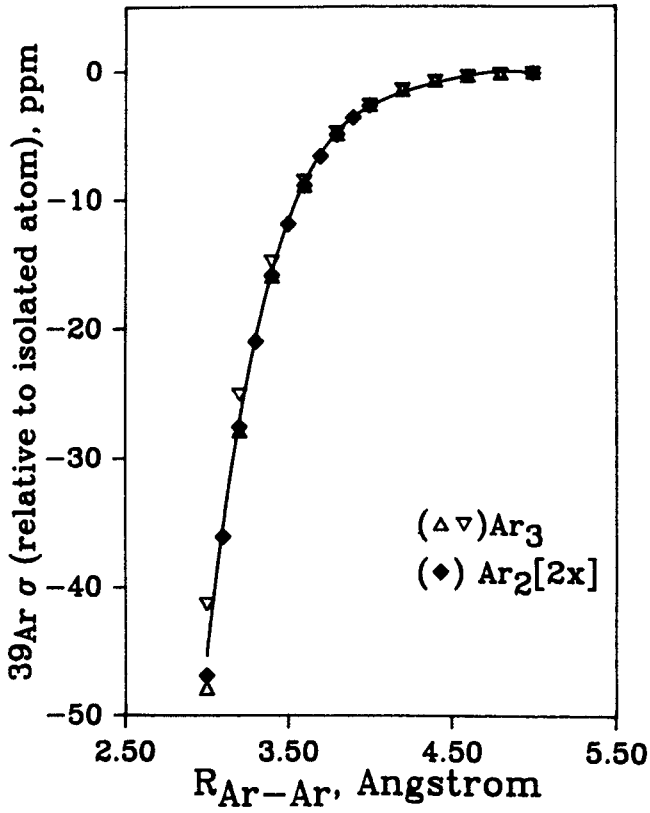

FIG. 17. In the range of Ar–Ar distances of interest, the intermolecular shielding is additive. Here we compare $2[\sigma(R)-\sigma(\infty)]_{Ar\text{-}Ar}$ (solid curve) with $[\sigma(R)-\sigma(\infty)]_{Ar_3}$ in the triangular and linear clusters.

tive. The triangular Ar_3 cluster is a reasonable model for the symmetrical arrangement of the three Xe atoms in the alpha cage, whereas the linear Ar–Ar–Ar is an unlikely configuration of three Xe atoms inside an alpha cage. What the linear Ar_3 does show is that the deshielding effect of the more remote Ar atom is considerably smaller than the effect of the nearest Ar atom in going from the dimer Ar–Ar to the trimer Ar–Ar–Ar. Furthermore, the ^{39}Ar nucleus in an argon atom interacting with two others (whether in a triangular or in a linear geometry) is deshielded compared to an argon atom interacting with only one. At very short range (not shown in Fig. 16), the geometry of the Ar_3 cluster (linear or triangular) is very important; the curves diverge with Ar in the triangular geometry experiencing a smaller negative shielding than the shielding of the central Ar in the linear geometry. However, at the intermediate distances which are of interest here, the ^{39}Ar shielding due to two neighbor Ar atoms becomes more nearly equal in the two types of geometries and, whether triangular or linear geometry, is nearly twice the shielding due to a single Ar neighbor. In Fig. 17, we show the *ab initio* ^{39}Ar shielding in Ar_2 after multiplication by 2.0 (solid curve and filled diamonds) compared with the ^{39}Ar shielding in the triangular (∇) and linear (Δ) Ar_3 clusters. For Ar–Ar distances greater than or equal to 3.0 Å, the *ab initio* values of the intermolecular shieldings in Ar_3 are nearly equal to twice the intermolecular shielding in Ar_2. Thus, the *ab initio* intermolecular shieldings are indeed very close to additive in the relevant range of Ar–Ar distances. At much shorter distances ($R < 3.0$ Å), deviations from additivity begin to appear. We might expect the intermolecular shielding in Ar_4, Ar_5, and Ar_6 to be nearly three, four, and five times $[\sigma(R)-\sigma(\infty)]_{Ar_2}$. This is in general agreement with the observed spectrum shown in Fig. 14. Using the ^{39}Ar model system, we reproduce the direction of the ^{129}Xe shifts and the near additivity that have been observed experimentally.

The slight increase in the incremental shifts in going from Xe_2 to Xe_6 can also be accounted for without postulating any perturbations of the incremental shieldings by the alpha cage environment other than confinement. As additional Xe atoms are introduced into the finite cavity size, the average Xe–Xe distances have to decrease. This implies that the range of Xe–Xe distances over which the averaging of the shielding takes place moves to shorter values. We note that in the Ar_2 dimer as well as in the two geometries of Ar_3, the ^{39}Ar shielding drops to larger negative values at shorter Ar–Ar distances. The ^{39}Ar model system would appear to lead to incremental ^{129}Xe chemical shifts that are increasing with the number of Xe atoms in the alpha cage, just as observed in experiment.

The average closest Xe–Xe distances will decrease as the cluster size increases since the confining cage has a rigid

structure. Molecular dynamics simulations show that sorbate molecules stay close to the wall of the alpha cage even at temperatures when skating from site to site along the inner surface of the cage occurs.[62–64,71,76,77] If the cavity is strictly spherical, energy calculations indicate that the Xe nuclei have the highest probability of being found within a spherical shell about 2.9 Å away from the oxygen atoms comprising the cavity.[71] The distances between neighboring Xe atoms in Xe_n, if the Xe atoms were distributed equally within this shell of radius R_e, would be $2R_e$, $3^{1/2}R_e$ $(8/3)^{1/2}R_e$, $2^{1/2}R_e$, and $2(3)^{-1/2}R_e$ for Xe_2, Xe_3, Xe_4, Xe_6, and Xe_8, respectively, corresponding to Xe–Xe distances ranging from about 8 to about 4.5 Å. However, the cavity is not spherical, so the available volume in the alpha cage is actually less than that for a spherical cavity. Furthermore, there is evidence that the average Xe–Xe distances are much shorter than these, the most probable Xe–Xe separations being closer to the $R_{\min}$ of the two-atom Xe–Xe potential. For example, molecular dynamics simulations of xenon atoms inside a zeolite *Y* cage (which is only slightly larger than a zeolite *A* alpha cage) show the main peak in the xenon–xenon radial distribution function at 4.5 Å. This suggests the existence of significant dimer formation even at the very low average xenon concentration of one xenon per cage.[65] This also suggests that the observed ^{129}Xe chemical shifts δ_2 and δ_3 would reflect averaging over those regions of the Xe_2 and Xe_3 shielding functions closest to 4.5 Å. The ^{39}Ar model shows us in Fig. 17 that as n increases, there is an incremental decrease in shielding for the *same* Xe–Xe distance in going from Xe_2 to Xe_3, which is very nearly the same as the decrease in going from Xe to Xe_2. This predicts nearly equal chemical shift increments. From the above discussion, we expect a further decrease in shielding as the number of xenon atoms in a cavity increases because the average Xe–Xe distance decreases too. This predicts slightly increasing chemical shift increments.

Another observation in the NMR spectra of xenon atoms trapped in zeolite Na*A* is the much larger decrease (about double) in ^{129}Xe chemical shielding in Xe_7 relative to Xe_6 (shown in Fig. 14), and in Xe_8 relative to Xe_7 (given in Ref. 14), as compared to the incremental decrease in shielding within the Xe_n series for $n = 1$–6. We see in Fig. 2 that the ^{39}Ar shielding in the Ar_2 dimer drops drastically with decreasing Ar–Ar distance. We found the same drastic decrease in shielding with decreasing Ar–Ar distance in the Ar_3 cluster (Fig. 16). Although we did not carry out the *ab initio* calculations for the larger Ar_n clusters, it is to be expected that each of the shielding functions for the Ar_n clusters will have the same dramatic drop in shielding with decreasing Ar–Ar distances. The serious overcrowding in cavities with seven or eight Xe atoms in the zeolite cage leads to averaging over a much narrower range of Xe–Xe distances and also much shorter Xe–Xe distances than for $n = 2$–6. These much shorter average Xe–Xe distances must therefore be associated with more drastically decreased average shielding than for $n = 2$–6.

Finally, we can also explain the observed temperature shifts of each of the Xe_n NMR signals. It was observed that a single Xe atom in an alpha cage showed a chemical shift decreasing with increasing temperature. This can be explained in terms of the one-particle distribution function within the alpha cage being sharply peaked at the minimum energy position about 2.9 Å from the oxygen atoms of the alpha cage. As the temperature increases, the one-particle distribution function spreads towards larger distances from the oxygen atoms. The Drude model gives the thermal average chemical shift of a single Xe atom in the cavity in Eq. (27). This leads to smaller δ_1 with increasing temperature. On the other hand, experimentally the larger clusters Xe_5 through Xe_8 show an increase in the chemical shift with increasing temperature, the temperature coefficient increasing with cluster size, the largest for Xe_7 and Xe_8. This is consistent with the increasing chemical shift increment with cluster size. Unlike in the gas phase, the confinement of xenon atoms by the alpha cage precludes averaging over larger Xe–Xe distances. However, for the larger occupancy numbers, where the range of the Xe–Xe distances are narrowed because of confinement, an increase in temperature increases the sampling of yet shorter Xe–Xe distances. If we take the shape of our *ab initio* shielding functions for Ar_2 and Ar_3 in Fig. 17 as typical of the higher Xe_n, we can sketch out the expected shielding functions for Xe_5 through Xe_8. In these functions, the enhanced sampling of the large negative shieldings (large positive chemical shifts) with decreasing Xe–Xe distances leads to the observed increase of the chemical shift with increasing temperature. A complete quantitative interpretation of the cluster shifts and their temperature dependence will require the radial distribution functions of xenon atoms in alpha cages containing from two up to eight xenon atoms. The latter can be provided by molecular dynamics simulations.

VII. CONCLUSIONS

We have determined the first *ab initio* intermolecular shielding function $[\sigma(R) - \sigma(\infty)]$ for a pair of interacting atoms for a wide range of internuclear separations using the localized orbital local origin (LORG) approach, including second-order electron correlation contributions (SOLO). We find that the ^{39}Ar shielding in Ar_2 and the ^{21}Ne shielding in Ne have qualitatively the same shapes; the curves are consistent with the large positive value at the united atom limit, go to zero at some very short distance, going through a minimum and asymptotically approaching zero at larger separations with a behavior that is close to, but not exactly R^{-6}. The minimum in the shielding is exhibited at separations much shorter than the van der Waals diameter for the pair, at separations that are well inside the distance corresponding to $V(R) = 0$. In the regions of R where $\exp[-V(R)/kT]$ weighting is significant, the intermolecular shielding function is negative and drops as roughly R^{-6}. Comparison with the intramolecular shielding function for a nucleus in a covalently bound diatomic molecule provides a unified view of intermolecular and intramolecular shielding. We show that conventional CHF calculations using a common gauge origin should not be used for this purpose; they give rise to an artifact—positive intermolecular shielding at large and intermediate distances.

The *ab initio* shielding function for Ar_2 provides the temperature dependence of the second virial coefficient of chemical shielding $\sigma_1(T)$, which reproduces the qualitative temperature behavior observed experimentally in gas phase NMR studies of ^{129}Xe in various gases.

It is found that an adequate shielding scaling factor for noble gases is provided by the quantity $\alpha_1(0)\langle a_0^3/r^3\rangle_1 \alpha_2(0)U_1U_2/(U_1+U_2)$, based on the Drude model, using the known static polarizabilities and ionization potentials. This factor allows the *ab initio* $[\sigma(R)-\sigma(\infty)]$ functions for ^{39}Ar in Ar_2 to be converted to the appropriate functions for ^{129}Xe in XeXe, XeKr, and XeAr in the regions of R that contribute significantly to the thermal average $\sigma_1(T)$ without having to use any adjustable parameters. Agreement with the experimental values is found to be satisfactory in all three cases. Furthermore, the *ab initio* ^{21}Ne shielding in Ne_2 agrees with the scaled *ab initio* ^{39}Ar in Ar_2 function in the same region of interest. The R values are scaled by the law of corresponding states, using the corresponding r_0 values for $V(R)$ of the interacting pairs.

Experimental observations of the chemical shifts of ^{129}Xe in Xe_n clusters in zeolite cavities are interpreted successfully with the help of *ab initio* intermolecular shielding calculations for ^{39}Ar in Ar interacting with Na^+ ion and ^{39}Ar in the Ar_3 cluster (linear and triangular geometries). The Drude model applied to a xenon atom in an idealized spherical cavity provides not only an approximate expression for the adsorption energy, but also the chemical shift of the single Xe atom in an alpha cage. With *ab initio* calculations on simple systems at the level which includes second-order electron correlation and a scaling up to large systems based on the Drude model, we have provided a reasonable theoretical interpretation of the ^{129}Xe chemical shifts of xenon atoms trapped in the alpha cages of zeolite Na*A*.

ACKNOWLEDGMENTS

We thank Professor T. D. Bouman for illuminating discussions relating to second-order electron correlation contributions to shielding and for his help in carrying out the SOLO calculations at Southern Illinois University, Edwardsville. This research has been supported by the National Science Foundation under Grant No. CHE-8901426.

[1] C. J. Jameson, Chem. Rev. **91**, 1375 (1991).
[2] C. J. Jameson, Bull. Magn. Reson. **3**, 3 (1980).
[3] J. Fraissard and T. Ito, Zeolites **8**, 350 (1988).
[4] H. Pfeifer, *NMR—Basic Principles and Progress* (Springer, Berlin, 1972), Vol. 7, p. 53; H. Pfeifer, W. Meiler, and D. Deininger, Annu. Rep. NMR Spectrosc. **15**, 291 (1983).
[5] R. A. Hegstrom, Phys. Rev. A **19**, 17 (1979).
[6] C. J. Jameson, J. Chem. Phys. **63**, 5296 (1975).
[7] J. P. Riley, I. H. Hillier, and W. T. Raynes, Mol. Phys. **38**, 353 (1979).
[8] K. Jackowski, W. T. Raynes, and A. J. Sadlej, Chem. Phys. Lett. **54**, 128 (1978).
[9] C. Giessner-Prettre and S. Ferchiou, J. Magn. Reson. **55**, 64 (1983).
[10] A. J. Sadlej, M. Zaucer, and A. Azman, Mol. Phys. **35**, 1397 (1978).
[11] M. Schindler and W. Kutzelnigg, J. Chem. Phys. **76**, 1919 (1982).
[12] C. J. Grayce and R. A. Harris, Mol. Phys. **71**, 1 (1990).
[13] C. J. Grayce and R. A. Harris, Mol. Phys. **72**, 523 (1991).
[14] C. J. Jameson, A. K. Jameson, R. Gerald II, and A. C. de Dios, J. Chem. Phys. **96**, 1676 (1992).
[15] A. D. Buckingham, T. Schaefer, and W. G. Schneider, J. Chem. Phys. **32**, 1227 (1960).
[16] F. H. A. Rummens, in *NMR Basic Principles and Progress*, edited by P. Diehl, E. Fluck, and R. Kosfeld (Springer, Berlin, 1975), Vol. 10.
[17] R. Eisenschitz and F. London, Z. Phys. **60**, 491 (1930).
[18] M. J. Stephen, Mol. Phys. **1**, 223 (1958).
[19] T. W. Marshall and J. A. Pople, Mol. Phys. **1**, 199 (1958).
[20] W. T. Raynes, A. D. Buckingham, and H. J. Bernstein, J. Chem. Phys. **36**, 3481 (1962).
[21] A. A. Bothner-By, J. Mol. Spectrosc. **5**, 52 (1960).
[22] J. O. Hirschfelder, C. F. Curtiss, and R. B. Bird, *Molecular Theory of Gases and Liquids* (Wiley, New York, 1954).
[23] F. London, Z. Phys. Chem. B **11**, 222 (1930), Trans. Faraday Soc. **33**, 8 (1937).
[24] A. D. Buckingham, Can. J. Chem. **38**, 300 (1960).
[25] F. M. Mourits, Ph.D. thesis, Regina, Canada, 1976.
[26] F. H. A. Rummens and F. M. Mourits, Can. J. Chem. **55**, 3021 (1977).
[27] A. E. Hansen and T. D. Bouman, J. Chem. Phys. **82**, 5035 (1985).
[28] J. Oddershede, P. Jørgensen, and D. L. Yeager, Comput. Phys. Rep. **2**, 33 (1984); J. Oddershede and J. R. Sabin, Int. J. Quantum Chem. **39**, 371 (1991).
[29] J. Oddershede and J. Geertsen, J. Chem. Phys. **92**, 6036 (1990).
[30] T. D. Bouman and A. E. Hansen, Chem. Phys. Lett. **175**, 292 (1990).
[31] R. D. Amos, Mol. Phys. **39**, 1 (1980).
[32] R. D. Amos, Chem. Phys. Lett. **68**, 536 (1979).
[33] C. J. Jameson, A. C. de Dios, and A. K. Jameson, J. Chem. Phys. **95**, 9042 (1991).
[34] C. J. Jameson, A. C. de Dios, and A. K. Jameson, J. Chem. Phys. **95**, 1069 (1991).
[35] M. J. Frisch, M. Head-Gordon, H. B. Schlegel, K. Raghavachari, J. S. Binkley, C. Gonzalez, D. J. Fox, R. A. Whiteside, R. Seeger, C. F. Melius, J. Baker, R. Martin, L. R. Kahn, J. J. P. Stewart, E. M. Fluder, S. Topial, and J. A. Pople, Gaussian, Inc., Pittsburgh, PA, 1988.
[36] T. D. Bouman, Southern Illinois University, Edwardsville, and Aa. E. Hansen, H. C. Oersted Institute, Copenhagen, Denmark.
[37] S. F. Boys and F. Bernardi, Mol. Phys. **19**, 553 (1970).
[38] G. C. Maitland, M. Rigby, E. B. Smith, and W. A. Wakeham, *Intermolecular Forces, Their Origin and Determination* (Clarendon, Oxford, 1981).
[39] T. D. Gierke and W. H. Flygare, J. Am. Chem. Soc. **94**, 7277 (1972).
[40] G. Malli and C. Froese, Int. J. Quantum Chem. Symp. **1**, 95 (1967).
[41] D. Kolb, W. R. Johnson, and P. Shorer, Phys. Rev. A **26**, 19 (1982).
[42] T. W. Marshall and J. A. Pople, Mol. Phys. **3**, 339 (1960).
[43] A. D. Buckingham and J. A. Pople, Discuss. Faraday Soc. **22**, 17 (1956).
[44] C. J. Jameson, A. K. Jameson, and S. M. Cohen, J. Chem. Phys. **65**, 3401 (1976).
[45] C. J. Jameson, A. K. Jameson, and H. Parker, J. Chem. Phys. **68**, 3943 (1978).
[46] C. J. Jameson and J. Mason, in *Multinuclear NMR*, edited by J. Mason (Plenum, New York, 1987), pp. 51–88.
[47] C. J. Jameson, A. K. Jameson, and S. M. Cohen, J. Chem. Phys. **59**, 4540 (1973).
[48] C. J. Jameson, A. K. Jameson, and S. M. Cohen, J. Chem. Phys. **62**, 4224 (1975).
[49] K. W. Miller, N. V. Reo, A. J. M. S. Uiterkamp, D. P. Stengle, T. R. Stengle, and K. L. Williamson, Proc. Natl. Acad. Sci. USA **78**, 4946 (1981).
[50] R. K. Mazitov, K. M. Enikeev, and A. V. Ilyasov, Z. Phys. Chem. **155**, 55 (1987).
[51] P. Diehl, O. Muenster, and J. Jokisaari, Chem. Phys. Lett. **178**, 147 (1991).
[52] B. B. Howard, B. Linder, and M. T. Emerson, J. Chem. Phys. **36**, 485 (1962).
[53] C. J. Jameson and H. J. Osten, Annu. Rep. NMR Spectrosc. **17**, 1 (1986).
[54] C. J. Jameson, A. K. Jameson, and P. M. Burrell, J. Chem. Phys. **73**, 6013 (1980).
[55] D. B. Chesnut, Chem. Phys. **110**, 415 (1986).
[56] P. J. Barrie and J. Klinowski, Prog. NMR Spectrosc. (in press).
[57] C. Dybowski, N. Bansal, and T. M. Duncan, Annu. Rev. Phys. Chem. **42**, 433 (1991).
[58] B. F. Chmelka, J. G. Pearson, S. B. Liu, R. Ryoo, L. C. de Menorval, and A. Pines, J. Phys. Chem. **95**, 303 (1991).
[59] L. C. de Menorval, D. Raftery, S. B. Liu, K. Takegoshi, R. Ryoo, and A. Pines, J. Phys. Chem. **94**, 27 (1990).

[60] A. Gedeon, T. Ito, and J. Fraissard, Zeolites **8**, 376 (1988).
[61] J. Pluth and J. V. Smith, J. Am. Chem. Soc. **102**, 4704 (1980).
[62] E. Cohen de Lara, R. Kahn, and A. M. Goulay, J. Chem. Phys. **90**, 7482 (1989).
[63] R. L. June, A. T. Bell, and D. N. Theodorou, J. Phys. Chem. **94**, 8232 (1990).
[64] G. B. Woods, A. Z. Panagiotopoulos, and J. S. Rowlinson, Mol. Phys. **63**, 49 (1988).
[65] S. Yashonath, Chem. Phys. Lett. **177**, 54 (1991).
[66] S. Yashonath, P. Demontis, and M. L. Klein, J. Phys. Chem. **95**, 5881 (1991).
[67] M. Schmeits and A. A. Lucas, Prog. Surf. Sci. **14**, 1 (1983).
[68] M. Schmeits and A. A. Lucas, J. Chem. Phys. **65**, 2901 (1976).
[69] E. G. Derouane, J. M. Andre, and A. A. Lucas, Chem. Phys. Lett. **137**, 336 (1987).
[70] R. Y. Yanagida, A. A. Amaro, and K. Seff, J. Phys. Chem. **77**, 805 (1973).
[71] I. Derycke, J. P. Vigneron, Ph. Lambin, A. A. Lucas, and E. G. Derouane, J. Chem. Phys. **94**, 4620 (1991).
[72] A. K. Jameson, C. J. Jameson, and H. S. Gutowsky, J. Chem. Phys. **53**, 2310 (1970).
[73] E. G. Derouane and J. B. Nagy, Chem. Phys. Lett. **137**, 341 (1987).
[74] E. G. Derouane, NATO ASI Ser. **221**, 225 (1989), *Guidelines for Mastering the Properties of Molecular Sieves* (Plenum, New York, 1989).
[75] E. G. Derouane, Chem. Phys. Lett. **142**, 200 (1987).
[76] G. B. Woods and J. S. Rowlinson, J. Chem. Soc., Faraday Trans. 2 **85**, 765 (1989).
[77] S. Yashonath, J. Phys. Chem. **95**, 5877 (1991).